

Evaluation of soil carbon simulation in CMIP6 Earth System Models

Rebecca M. Varney¹, Sarah E. Chadburn¹, Eleanor J. Burke², and Peter M. Cox¹

¹College of Engineering, Mathematics and Physical Sciences, University of Exeter, Laver Building, North Park Road, Exeter, EX4 4QF, UK

²Met Office Hadley Centre, FitzRoy Road, Exeter, EX1 3PB, UK

Correspondence: Rebecca M. Varney (r.varney@exeter.ac.uk)

Abstract.

The response of soil carbon represents one of the key uncertainties in future climate change. The ability of Earth System Models (ESMs) to simulate present day soil carbon is therefore vital for reliably estimating global carbon budgets required for Paris agreement targets. In this study CMIP6 ESMs are evaluated against empirical datasets to assess the ability of each model to simulate soil carbon and related controls: Net Primary Productivity (NPP) and soil carbon turnover time (τ_s). Comparing CMIP6 with the previous generation of models (CMIP5), a lack of consistency in modelled soil carbon remains, particularly the underestimation of northern high latitude soil carbon stocks. There is a robust improvement in the simulation of NPP in CMIP6 compared with CMIP5, however an unrealistically high correlation to soil carbon stocks remains, suggesting the potential for an overestimation of the long-term terrestrial carbon sink. Additionally, the same improvements are not seen in the simulation of τ_s . These results suggest much of the uncertainty associated with modelled soil carbon stocks can be attributed to the simulation of below ground processes, and greater emphasis is required on improving the representation of below ground soil processes in future developments of models. These improvements would help reduce the uncertainty in projected carbon release from global soils under climate change and to increase confidence in the carbon budgets associated with different levels of global warming.

1 Introduction

Soil carbon is the Earth's largest terrestrial carbon store, with a magnitude of at least three times the amount of carbon contained within the atmosphere (Jackson et al., 2017). The response of soil carbon to CO₂-induced global warming has the potential to provide a significant feedback on climate change, but this feedback is currently poorly known (Friedlingstein et al., 2006; Gregory et al., 2009; Arora et al., 2013; Friedlingstein et al., 2014; Arora et al., 2020; Song et al., 2021). Carbon stored within the atmosphere and global soils is exchanged via carbon fluxes, as part of the global carbon cycle (Canadell et al., 2021). The Earth's terrestrial surface has acted as a carbon sink until now (Pan et al., 2011), but there is a possibility of a switch to a source during the 21st century, which would accelerate climate change (Cox et al., 2000; Crowther et al., 2016). Due to the significant quantities of carbon stored in soils globally, understanding and quantifying the potential release of carbon from soils is vital if the existing Paris Agreement Targets are to be met (UNFCCC, 2015).

25 Earth System Models (ESMs) are complex numerical models which simulate both climate and carbon cycle processes, and are used to make projections of climate change. The latest generation of the Coupled Model Intercomparison Project (CMIP) CMIP6 (Eyring et al., 2016), includes an ensemble of ESMs, which are used in the most recent Intergovernmental Panel on Climate Change (IPCC) report (AR6) (IPCC, 2021). The relationships between carbon and environmental drivers used in models help to determine the response of the carbon cycle to climate change (Todd-Brown et al., 2013). Therefore, representing
30 present day carbon stores and spatial controls realistically within models is key for estimating carbon emission cuts required for Paris agreement targets (Friedlingstein et al., 2022).

Present day soil carbon can be approximately broken down into above ground and below ground controls, which influence the spatial distribution of soil carbon stocks (Koven et al., 2015). The above ground control of soil carbon can be considered as the input flux of carbon into the soil from vegetation. Both the amount of carbon from plant and root litter (known as litterfall),
35 and the fraction of this that is converted to longer-lived soil carbon pools, will influence the storage of soil carbon. Net Primary Productivity (NPP) can be used as a proxy for the litterfall flux, where the fluxes are equal when vegetation is in a steady state. The below ground control of soil carbon can be quantified simply in terms of the soil carbon turnover time (τ_s), which is defined as the time carbon resides in the soil (Koven et al., 2017; Carvalhais et al., 2014). τ_s can be considered as a proxy for below ground controls on soil carbon storage (Koven et al., 2015).

40 In this study, the representation of late 20th century soil carbon stores and these related controls (NPP and τ_s) are evaluated in CMIP6 ESMs. Previously, similar studies have been conducted to evaluate soil carbon in the preceding generations of ESMs, for example: Anav et al. (2013) and Todd-Brown et al. (2013) for CMIP5. There are some existing CMIP6 soil carbon related studies, for example: Arora et al. (2020) evaluate carbon-concentration and carbon-climate feedbacks in 1% CO₂ per year forcing simulations, Burke et al. (2020) evaluates the representation of permafrost in models, and Ito et al. (2020) investigate
45 future soil carbon stocks under specific land-use conditions. This study is the first to specifically focus on global and spatial soil carbon and related controls in CMIP6, with a thorough evaluation against empirical datasets and comparison against the preceding CMIP5 ensemble.

2 Methods

2.1 Earth system models

50 Soil carbon stores and related controls are examined in eleven CMIP6 ESMs (Eyring et al., 2016; Meehl et al., 2014), as listed in Table 1. Throughout the study, comparisons are made with ten ESMs from the previous CMIP generation (CMIP5, Taylor et al. (2012)), as listed in Table 2. The ESMs included in this study were chosen due to the availability of the required data in the online repository at the time of analysis (<https://esgf-node.llnl.gov/search/cmip6/>, <https://esgf-node.llnl.gov/search/cmip5/>).

Tables 1 (CMIP6) and 2 (CMIP5) present information about the included ESMs, specifically more details about the associated Land Surface Model (LSM). It should be noted that there are similarities between some of the LSMs - either advances from earlier models, or even the same LSM within different ESMs. For example, CESM2 and NorESM2-LM both use the Community Land Model version 5 (CLM5) (Arora et al., 2020). For some modelling centres, both the CMIP5 and CMIP6

versions of the models are included, and in these cases direct comparisons can be made to determine changes from CMIP5 to CMIP6. These generationally related CMIP5 and CMIP6 models are: CanESM2 and CanESM5, CCSM4 and CESM2, 60 GFDL-ESM2G and GFDL-ESM4, IPSL-CM5A-LR and IPSL-CM6A-LR, MIROC-ESM and MIROC-ES2L, MPI-ESM-LR and MPI-ESM1.2-LR, NorESM1-M and NorESM2-LM, and HadGEM2-ES and UKESM1-0-LL, respectively. The models where only either the CMIP5 or CMIP6 version from the modelling centre was included are: BNU-ESM and GISS-E2-R from CMIP5 and ACCESS-ESM1.5, BCC-CSM2-MR and CNRM-ESM2-1 from CMIP6. A key general change to note is that CMIP6 has more models that include an interactive nitrogen cycle compared with CMIP5: ACCESS-ESM1.5, CESM2, 65 MIROC-ES2L, MPI-ESM1.2-LR, NorESM2-LM and UKESM1-0-LL in CMIP6 compared with CCSM4 and NorESM1-M in CMIP5. (The CMIP5 model BNU-ESM includes carbon-nitrogen interactions, however this process was turned off in CMIP5 simulations (Ji et al., 2014)). Additionally, an increased number of soil carbon pools is seen in some CMIP6 models (e.g. CLM5 has 29 carbon pools compared with 20 in CLM4). Arora et al. (2020) include a comprehensive overview of the updates seen in the individual CMIP6 models, which is presented in the ‘Model descriptions’ section of the associated Appendix.

70 Todd-Brown et al. (2013) include a summary of the temperature and moisture dependencies of soil respiration/decomposition as assumed in the CMIP5 models (see Table 1 of the Todd-Brown et al. (2013) study). The most common representation of the temperature sensitivity of decomposition is the Q_{10} equation, which is defined by $f(T) = Q_{10}^{(T-T_0)/10}$, where T is temperature and T_0 is a reference temperature. With the Q_{10} equation, decomposition increases exponentially with temperature (Davidson and Janssens, 2006). The majority of other models used the Arrhenius equation to represent the temperature sensitivity, where 75 the main difference from the Q_{10} representation is that decomposition levels off at higher temperature levels (Lloyd and Taylor, 1994). Of the remaining models, the GFDL model simulates an increased decomposition with temperature until some optimal temperature above which it decreases (Shevliakova et al., 2009) (which Todd-Brown et al. (2013) defined as a ‘hill’ function) and the GISS model implement a linear increase of respiration to temperature up to a maximum value (Del Grosso et al., 2005). The representation of the decomposition sensitivity to soil moisture was found to be to be represented in two ways amongst 80 the CMIP5 models, where either decomposition was assumed to increase monotonically with increasing soil moisture, or less commonly to increase to some optimum moisture level and then decrease (again described as a ‘hill’ function by Todd-Brown et al. (2013)). In this study we note that the representation of temperature and moisture functions remain similar from CMIP5 from CMIP6. The Q_{10} equation remains the most common representation of soil temperature sensitivity in models, followed by the Arrhenius equation and then ‘hill’ functions. Similarly, the most common representation of the sensitivity of soil to 85 moisture in CMIP6 is a monotonically increasing function, followed by ‘hill’ functions of various sorts.

2.2 Defining soil carbon variables

CMIP defines common output variables (Meehl et al., 2000), which allows for consistent comparison between the models, and for cleaner evaluation of models against observational data. These common output variables also allow for consistent comparison between model generations, in this case between CMIP6 and CMIP5. This study focuses on evaluation of near 90 present day soil carbon and related controls. Therefore the results presented in this study use the CMIP standard historical simulation (CMIP scenario *historical*), for both the CMIP6 and CMIP5 analysis. The historical simulation runs from 1850 to

2015 in CMIP6 and from 1850 to 2005 in CMIP5, where the selected dates for each variable (stated below) were chosen to allow for consistent comparison between CMIP5 and CMIP6, and to best match the modelled data to the observational data.

To evaluate soil carbon, this study uses ‘Soil Carbon’ (CMIP variable *cSoil*) which represents the carbon stored in soils, and where applicable ‘Litter Carbon’ (CMIP variable *cLitter*) which represents carbon stored in the vegetation litter. Total soil carbon (C_s) is defined to be the sum of these soil carbon and litter carbon variables ($cSoil + cLitter$), where for models that do not report a separate litter carbon pool, the total soil carbon is taken to be simply the *cSoil* variable. This allows for a more consistent comparison between the models and between the models and empirical data, due to differences in how soil carbon and litter carbon are simulated (Todd-Brown et al., 2013; Arora et al., 2020). Modelled C_s is time averaged between the years 1950 to 2000 of the historical simulation, and is considered spatially (units of kg m^{-2}), and as global totals (units of PgC), where global totals are calculated as an area weighted sum using the model land surface fraction (CMIP variable *sflf*). To calculate northern latitude totals, a sum between the latitudes 60° N and 90° N is considered.

The CMIP6 ESMs CESM2 and NorESM2-LM have two different variables to represent soil carbon: (1) CMIP variable *cSoil*, which represents the full vertical soil profile, and (2) CMIP variable *cSoilAbove1m*, which represents soil carbon in the top 1m of soil. This is due to the representation of vertically resolved soil carbon in these models, which means there are separate carbon pools in the model that represent different soil depths (Lawrence et al., 2019). The CMIP variable *cSoilAbove1m* is used throughout this study to represent soil carbon for the models CESM2 and NorESM2-LM, unless otherwise stated. The use of this variable is to enable a more consistent comparison with both the other CMIP6 models and the CMIP5 models. Therefore, an assumption of a 1m depth of soil for modelled soil carbon allows for the fairest evaluation, and evaluation is considered against empirical datasets down to a depth of 1m (see below). However, comparisons with the *cSoil* variable for both CESM2 and NorESM2-LM are included in Tables 4 and 6 of the Results.

In order to obtain a clean separation between above ground and below ground drivers of soil carbon variations, a quasi-equilibrium approximation is made. We begin with the definition of the effective soil carbon turnover time (τ_s) (Varney et al., 2020; Koven et al., 2017; Carvalhais et al., 2014), which represents the average time carbon resides in the soil:

$$\tau_s = \frac{C_s}{R_h} \quad (1)$$

where R_h is the output flux of carbon from the soil known as the heterotrophic respiration, which is described as the carbon loss from the decomposition by microbes. This definition of the turnover time implicitly neglects other processes that results in soil carbon release, but which are not yet routinely included in ESMs (e.g. peat fires or dissolved organic carbon fluxes).

The definition of the effective turnover time (Eq. 1) ensures that the soil carbon at any one time is given by: $C_s = R_h \tau_s$. In an unperturbed steady-state (i.e. neglecting disturbances from land-use change, fires, insect outbreaks etc.), there is no net exchange of carbon between land and atmosphere, and therefore R_h is equal to litterfall, known as fallen organic material from plants. When vegetation and soil carbon are close to a steady state, litterfall and R_h are also approximately equal to Net Primary Productivity (NPP), where NPP is defined as the net carbon assimilated by plants via photosynthesis minus loss due to plant respiration. In the contemporary period considered in this study, R_h has been found to be well approximated by NPP (Varney et al., 2020). This is because the difference between NPP and R_h , which represents the Net Ecosystem Productivity

(NEP), is a small fraction of the NPP over the historical period ($NPP \approx 60 \text{ PgC yr}^{-1}$; $NEP \approx 3 \text{ PgC yr}^{-1}$). Therefore the present day soil carbon can be approximated by:

$$C_s \approx NPP \tau_s \quad (2)$$

to a good accuracy. This allows for a clean separation of soil carbon variation into the above (NPP) and below (τ_s) ground
130 drivers of soil carbon spatial patterns, following the approach of previous published studies (Todd-Brown et al., 2013; Koven
et al., 2015).

To evaluate these soil carbon controls on C_s , NPP and τ_s are evaluated separately. This study uses modelled ‘Net Primary
Productivity’ (CMIP variable npp), which is defined as the mass flux of carbon out of the atmosphere due to NPP on land.
NPP is also considered spatially ($\text{kg m}^2 \text{ yr}^{-1}$), and as an area weighted global total flux (PgC yr^{-1}). By definition τ_s is defined
135 by Eq. 1, and therefore is calculated by soil carbon (as defined above) divided by R_h . For R_h , the variable ‘Heterotrophic
Respiration’ (CMIP variable rh) is used, which is defined as the mass flux of carbon into the atmosphere due to heterotrophic
respiration on land, primarily due to the microbial respiration that occurs in the soil, and where the units of R_h are the same
as that of NPP. The carbon fluxes (NPP and R_h) are time averaged over the period 1995 to 2005 for consistency between
the CMIP generations and to match the empirical datasets. τ_s can be considered on a spatial level, or as an effective global
140 τ_s , which is defined as average $\tau_s = \text{mean}(C_s) / \text{mean}(R_h)$ (where the mean represents an area weighted global average). The
advantage of defining an effective global τ_s is that it is not dominated by large spatial outlying values. Using either method,
the units for τ_s are in years (yr) by definition.

The relationships of C_s , NPP and τ_s , with both temperature and soil moisture are also considered. For temperature, the
variable ‘near surface air temperature’ (CMIP variable tas), representing atmospheric temperature at the surface is considered,
145 where the dates 1995 to 2005 were chosen to be consistent with the carbon fluxes. The variable for atmospheric temperature
is considered opposed to soil temperature as equivalent global observational datasets are required for the analysis. For soil
moisture, the variable ‘Moisture in Upper Portion of Soil Column’ (CMIP variable $mrsos$), which is defined as the mass
content of water in the soil layer in the upper portion of the soil (0-10cm depth) is considered, where the dates 1978 to 2000
were considered to match the empirical data. The standard output $mrsos$ is in units of kg m^2 , however in this study a volumetric
150 soil moisture, referred to as θ , is used to allow for consistent comparison with the benchmark data. θ is calculated as $mrsos$
divided by the depth of the soil layer in mm, which in this case is $\theta = mrsos/100$.

The variable $mrsos$ for soil moisture was considered opposed to the full soil column moisture (CMIP variable $mrs0$) as this
better matched the available empirical dataset for soil moisture. It is noted that this represents surface soil moisture and does
not match the depth over which soil carbon is evaluated (0-1m). This is due to deeper soil moisture products not being as
155 readily available due to limitations of remote sensing methods in penetrating deeper ground. It is expected that the surface soil
moisture will be related to deeper soil moisture to some extent but will be influenced by different processes. For example, high
surface soil moisture after rainfall events could run off and thus not always reach the deeper soil. However, due to the long
timescales considered (1978 - 2000) for both the modelled and empirical data, the average surface soil moisture will be closely
related to deeper moisture.

160 2.3 Empirical datasets

2.3.1 Soil carbon

Observational C_s to a depth of 1m was obtained by combining the empirical Harmonized World Soils Database (HWSD) (FAO and ISRIC, 2012) and Northern Circumpolar Soil Carbon Database (NCSCD) (Hugelius et al., 2013) soil carbon datasets, where NCSCD was used where overlap of the datasets occurs. This is a commonly used method when considering empirical
165 soil carbon and has been previously used in multiple studies, such as: Varney et al. (2020), Koven et al. (2017), and Todd-Brown et al. (2013). This dataset is referred to here as the ‘Benchmark dataset’.

We use the 95% confidence intervals given by Todd-Brown et al. (2013), to derive standard deviations about the global mean soil carbon. To do this, the constructed 95% confidence intervals were used to calculate upper and lower bounds around the mean value. Then assuming the data is normally distributed, these derived 95% confidence intervals were halved to obtain
170 confidence intervals equivalent to a standard deviation error on the mean (1412 ± 215 PgC). The uncertainty analysis completed in Todd-Brown et al. (2013) is used for the benchmark soil carbon dataset as no quantitative uncertainty has been previously or since defined for the HWSD and NCSCD datasets (Anav et al., 2013).

Additionally, the benchmark dataset was compared with empirical estimates found in the literature to improve the robustness and reliability of the evaluation. Todd-Brown et al. (2013) find that this derived uncertainty is consistent with other empirical
175 estimates of global soil carbon; for example, 1576 PgC in Eswaran et al. (1993), 1220 PgC in Sombroek et al. (1993), and 1502 PgC in Jobbágy and Jackson (2000). This study further compares with empirical estimates of 1395 PgC in Post et al. (1982) and 1515 PgC in Raich and Schlesinger (1992). These empirical estimates are within one standard deviation of the global mean soil carbon given by the benchmark dataset (Table 3).

Moreover, additional empirical datasets are considered to improve the reliability of the benchmark dataset (Table 3). These
180 additional datasets include: (1) the World Inventory of Soil property Estimates (WISE30sec) dataset down to a depth of 2m (Batjes, 2016), which includes a given standard deviation on the global total soil carbon consistent with our derived benchmark uncertainty, (2) the named ‘S2017’ from Sanderman et al. (2017) soil carbon estimate (1m and 2m), which uses a data-driven statistical model and the History Database of the Global Environment (HYDE) land use data, (3) the Global Soil Dataset for use in Earth System Models (GSDE), which provides a estimates for observational soil carbon down to a depth of up to 2.3m
185 (Shangguan et al., 2014), and (4) the Global Gridded Surfaces of Selected Soil Characteristics (IGBP-DIS) estimate of soil carbon to a depth of 1m, derived by the Oak Ridge National Laboratory Distributed Active Archive Centre (ORNL DAAC) (IGBP, 2000). These datasets were combined to obtain a mean estimate for observational soil carbon down to a depth of 1m, where a global total soil carbon value of 1560 ± 214 PgC was found. This estimate is consistent with our benchmark dataset estimate, and further improves the confidence in our benchmark soil carbon estimate.

190 Furthermore, the spatial correlation coefficients between these additional datasets and our benchmark dataset are considered, where the following values correspond to the above datasets: (1) 0.554, (2) 0.625, (3) 0.482, and (4) 0.622. Map plots comparing the empirical soil carbon datasets are shown in Fig. A1. The estimate for northern latitude total soil carbon has greater uncertainties associated with it, where the standard deviation deduced by combining the empirical datasets is 83 PgC.

To account for this increased uncertainty in these regions, the deduced standard deviation of 83 PgC is used on the benchmark
195 soil carbon throughout this study, opposed to the 61 PgC derived using the Todd-Brown et al. (2013) uncertainty analysis.

2.3.2 Carbon fluxes

To estimate a benchmark NPP, the commonly used MODIS NPP (2000-2010) dataset (Zhao et al., 2005) is used. The MODIS
NPP dataset does not have associated uncertainty estimates, so this study estimates a standard deviation error on benchmark
NPP as derived by Ito (2011). The MODIS NPP dataset is found to be consistent with 251 empirical present day estimates
200 of NPP found in the literature, which Ito (2011) used to estimate a global value of 56.2 ± 14.3 PgC yr⁻¹ (compared with
a derived MODIS mean value of 56.6 yr⁻¹). Moreover, due to the limited choice of observational derived NPP datasets
(Harper et al., 2018), models can be further evaluated against using a benchmark dataset for R_h , where R_h is estimated using
the CARDAMOM (2001–2010) heterotrophic respiration dataset (Bloom et al., 2015). The empirical CARDAMOM R_h has
associated estimates of error, which were used to derive a standard deviation uncertainty on the empirical average R_h ($51.7 \pm$
205 21.8 PgC yr⁻¹). This study includes map plots comparing the two empirical datasets, which is shown in Fig. A2. Global totals
for R_h are also considered for comparison against NPP, where the CMIP6 and CMIP5 values are also shown in Appendix
Tables A1 and A2, respectively.

2.3.3 Soil carbon turnover time

To estimate a benchmark τ_s , the estimates of observational C_s are divided by an estimate of R_h (see above). To estimate
210 an uncertainty on effective global τ_s , this study derived upper (τ_s^+) and lower (τ_s^-) bounds based on the derived C_s and R_h
uncertainty estimates. The upper bound was calculated using the following: $\tau_s^+ = C_s^+ / R_h^-$, where C_s^+ is equal to the mean
soil carbon plus one standard deviation and R_h^- is equal to the mean heterotrophic respiration minus one standard deviation.
The lower bound was calculated using the following: $\tau_s^- = C_s^- / R_h^+$, where similarly C_s^- is equal to the mean soil carbon
minus one standard deviation and R_h^+ is equal to the mean heterotrophic respiration plus one standard deviation. This method
215 gives a large uncertainty bound around the derived mean estimate (27.0_{-11}^{+27} yr), so the benchmark data is further compared to
empirical estimates. Raich and Schlesinger (1992) derive an estimate of mean soil carbon turnover of 32 yr, using estimates for
mean soil carbon pools and mean soil respiration rates. More recently, Carvalhais et al. (2014) derive an estimate for the mean
global ecosystem carbon turnover time of 23_{-4}^{+7} , which is a spatially explicit and observation based estimate. Ito et al. (2020)
derived an observational uncertainty range on soil carbon turnover time of 18.5 to 45.8 years, which was derived using similar
220 empirical estimates found in the literature. These estimates give more certainty on the values closer to the derived empirical
mean value for τ_s .

2.3.4 Soil moisture and air temperature

To estimate soil moisture (θ), the Copernicus Climate Change Service (C3S) ‘Soil moisture gridded data from 1978 to present’
dataset (published 2018-10-25) is used, where the years 1978 to 2000 are considered. This dataset is based on the ESA Climate

225 Change Initiative soil moisture, and estimates global surface soil moisture from a large set of satellite sensors (Copernicus
Climate Change Service, 2021; Liu et al., 2011, 2012; Wagner et al., 2012; Gruber et al., 2017; Dorigo et al., 2017). The
WFDEI Meteorological Forcing dataset is used to represent observational air temperatures (1995-2005) (Weedon et al., 2014),
where dates are chosen to allow for consistency between CMIP generations. This study includes no uncertainty analysis on
the soil moisture and air temperature empirical datasets as these datasets are only used to evaluate spatial correlations between
230 variables and not to evaluate soil moisture and air temperature in the models.

2.4 Regridding

To allow direct comparisons between the empirical data and model output data, the model data was regridded to match the
observational grid. In this case, the observational grid is a 0.5° by 0.5° resolution, 720 longitude and 360 latitude grid. The
regridding was done using Iris - the community-driven Python package for analysing and visualising Earth science data (Met
235 Office, 2010 - 2013). The regridding method assumed conservation of mass and used linear extrapolation, where extrapolation
points will be calculated by extending the gradient of the closest two points. Moreover, model land masks are used to calculate
the fraction of land in each coastal grid cell (CMIP variable *sftlf*).

2.5 Statistical analysis

It is difficult to evaluate the spatial distributions of modelled soil carbon and related spatial controls against empirical data
240 with a single metric, so the evaluation for both CMIP6 and CMIP5 involves multiple methods. These include: coefficients of
variation, spatial standard deviations, spatial Pearson correlation coefficients and Root Mean Square Errors (RMSEs). These
methods can be combined to give a more thorough evaluation of spatial soil carbon and associated controls in the CMIP6
models compared to the previous generation of CMIP5 models.

The coefficient of variation is defined as the ratio of the ensemble standard deviation (std) to the ensemble mean in each grid
245 cell. This is used to show the amount of variability amongst the models in the ensemble scaled to the size of the ensemble mean,
so represents the variability spatially in the ensemble and shows how much variation is present across the ensemble in specific
regions. It is presented as hatching on a map figure (Fig. 3), where shaded 'hatched' regions show regions of high variability
within the ensemble. These regions show areas where there is disagreement in the ensemble as there is large spread compared
with the mean, and was defined as where $std/mean > 0.75$. The regions where spatial $C_s < 5 \text{ kg m}^2$ were discounted as the
250 low values of soil carbon are present in these regions.

The spatial standard deviation is a measure of the spread in the data across the globe compared to the mean value. Pearson
correlation coefficients (r-values) were used as a spatial measure of the linear correlation between the empirical and modelled
data, where a high r-value (near 1 or -1) represents a high correlation in the data and a low r-value (near 0) represents a
negligible correlation. RMSE were used as an absolute measure of the difference between the modelled data and empirical
255 data, where the lower the value the lower the difference error. The RMSE can be considered as the standard deviation of the
difference, and it is a measure to show the deviation of the modelled data in relation to the empirical data. This statistical data:
spatial standard deviations, Pearson correlation coefficients, and RMSEs, can be presented using a Taylor diagram. A Taylor

diagram is a mathematical graph used to indicate the performance of a model compared with a benchmark, which in this case is the empirical datasets (Taylor, 2001).

260 3 Results

3.1 Soil carbon stocks: *northern latitude underestimations remain in CMIP6*

3.1.1 Global total evaluation

Global total soil carbon (in the top 1m of soil) is shown to vary amongst the ESMs in CMIP6, with a range of 1294 PgC between the models with the lowest and the highest values (Table 4). The global total soil carbon for two (CanESM5 and MIROC-ES2L) out of the eleven CMIP6 models falls within the benchmark soil carbon uncertainty range, 1197 - 1627 PgC (mean \pm stand deviation). The models with the largest global total soil carbon are CNRM-ESM2-1 (1810 PgC), BCC-CSM2-MR (1770 PgC), and UKESM1-0-LL (1760 PgC), values greater than the benchmark dataset but not the additional empirical datasets (Table 3). The models GFDL-ESM4 (516 PgC) and IPSL-CM6A-LR (639 PgC) have the lowest global total soil carbon values in the ensemble, with global totals significantly lower (approximately 50% less) than the global totals seen in empirical data. It is noted that if the full soil carbon profile is considered for CESM2 and NorESM2-LM opposed to a depth of 1m, the global total soil carbon values are increased to 1870 PgC from 991 PgC in CESM2, and to 2430 PgC from 969 PgC in NorESM2-LM.

Both the CMIP5 and CMIP6 ensemble mean global totals fall within the benchmark uncertainty range (Tables 4 and 5). The ensemble mean global total soil carbon is found to have reduced in CMIP6 from CMIP5 (1206 ± 445 PgC Vs 1480 ± 810 PgC). However, a significant reduction is seen in the associated standard deviation of the ensemble mean global totals is seen in CMIP6 compared with CMIP5 (± 445 PgC in CMIP6 from ± 810 PgC in CMIP5) and a reduced range of global total values (a range of 1294 PgC is seen in CMIP6 opposed to 2493 PgC in CMIP5). This suggests that although a significant range in global soil carbon still exists amongst the CMIP6 ESMs, there is an improved consistency between the models seen in CMIP6 compared with the models in CMIP5. Although it is noted that this may be a factor of the selection of models included in each ensemble rather than any change in process representation.

It is found from comparing the previous generation models in CMIP5 with the updated CMIP6 equivalent, that multiple models in CMIP6 have lower quantities of soil carbon than in CMIP5, such as: GFDL-ESM4 from GFDL-ESM2G, IPSL-CM6A-LR from IPSL-CM5A-LR, MIROC-ES2L from MIRCO-ESM and MPI-ESM1.2-LR from MPI-ESM-LR. For example, the CMIP5 model MPI-ESM-LR is reported to have the largest soil carbon magnitude amongst the CMIP5 models, with a global total of 3000 PgC (Table 5), whereas the updated CMIP6 model MPI-ESM1.2-LR has a reduced global total soil carbon value of 970 PgC, amongst the lowest values reported in CMIP6 and below observational derived range (Table 4). Conversely, these reductions are negated in the ensemble mean by the remaining models which have greater quantities of soil carbon in CMIP6 compared to their CMIP5 equivalent, such as CanESM5 from CanESM2, CESM2 from CCSM4, NorESM2-LM from NorESM1-M and UKESM1-0-LL from HadGEM2-ES. For example, the CMIP5 model NorESM1-M is amongst the lowest

soil carbon values presented in this ensemble at 538 PgC (Table 5), whereas the updated CMIP6 model NorESM2-LM has an
290 increased global total of 969 PgC (down to 1m) (Table 1).

3.1.2 Northern latitude total evaluation

Northern latitude soil carbon (down to a depth of 1m, and where northern latitudes defined as 60° N - 90° N) is found to be underestimated in CMIP6, with eight out of the eleven CMIP6 models having lower northern latitude soil carbon values than the derived observational range (Table 4). Two out of eleven CMIP6 models (CNRM-ESM2-1 and MIROC-ES2L) have northern
295 latitude totals that fall within the uncertainty range derived from the benchmark data, 318 - 484 PgC (mean \pm stand deviation). The CMIP6 models with the greatest northern latitude total soil carbon are BCC-CSM2-MR (575 PgC), CNRM-ESM2-1 (440 PgC), and MIROC-ES2L (347 PgC). The CMIP6 models with the lowest northern latitude soil carbon are IPSL-CM6A-LR (66 PgC), ACCESS-ESM1.5 (151), GFDL-ESM4 (163 PgC), MPI-ESM1.2-LR (175 PgC) and UKESM1-0-LL (194), values significantly lower than the totals seen in empirical data.

300 The northern latitude soil carbon total was also underestimated in CMIP5, with six out of the ten CMIP5 models estimating northern latitude totals lower than the empirical estimates (Table 5). The ensemble mean total northern latitude soil carbon is lower in CMIP6 (266 ± 139 PgC seen in Table 4) than in CMIP5 (318 ± 246 PgC seen in Table 5), which is consistent with the global total results, however both the CMIP5 and CMIP6 mean values fall below the benchmark range. Similarly, as with global soil carbon, a smaller standard deviation on the mean is found for CMIP6 compared with CMIP5 and there is a reduced
305 range in simulated northern latitude total values amongst the CMIP6 models, where despite a large range seen (66 to 575 PgC), an even greater range is seen in CMIP5 (28.1 to 742 PgC). Moreover, improvements are seen amongst models from CMIP5 to CMIP6. For example, the CMIP5 model NorESM1-M had a northern latitude total soil carbon value of 31.0 PgC, which is significantly lower than what is expected based on the benchmark dataset (Table 5). However, the updated CMIP6 version of this model, NorESM2-LM, has a northern latitude total soil carbon value of 300 PgC, which is much more in line with
310 the expected observational values (Table 4). An improved representation of northern latitude soil carbon is also seen CESM2 (compared with CCSM4), which has the same land surface model as NorESM2-LM (CLM5 (Lawrence et al., 2019)).

The CMIP6 models with the lowest global total values for soil carbon do not always correspond with the lowest northern latitude values for soil carbon. For example, UKESM1-0-LL global total soil carbon is amongst the highest global totals seen in CMIP6, however low quantities of soil carbon are seen in the northern latitudes (approximately 10% of the global total).
315 Conversely, BCC-CSM2-MR, CESM2, GFDL-ESM4, and NorESM2-LM have approximately 30% of their global total stocks in the northern latitude region, which is consistent with the ratio seen in the benchmark dataset. This result suggests that representing global total soil carbon stocks consistent with the benchmark soil carbon, does not imply the consistency in the representation of northern latitude soil carbon stocks, and these should be evaluated separately. However, the large uncertainties associated with the empirical datasets for the northern latitudes are noted (Table 3).

320 3.1.3 Spatial evaluation

A lack of consistency in the simulation of soil carbon was found amongst the CMIP5 models, which can be seen in Fig. 1(a), where differences between the empirical and modelled data is shown. Northern latitude soil carbon was found to be underestimated in CMIP5, where areas of blue can be seen in the northern latitudes of the CMIP5 soil carbon map in Fig. 1(a). This underestimation of CMIP5 northern latitude soil carbon is accompanied by significant overestimations seen in mid-
325 latitude soil carbon. Specifically, large quantities of soil carbon which are inconsistent with our benchmark dataset can be seen in the mid-latitude regions in the following CMIP5 models: CanESM2, GFDL-ESM2G, GISS-E2-R, MIROC-ESM, and MPI-ESM-LR, and less significant overestimations are seen in HadGEM2-ES and IPSL-CM5A-LR (Fig. A3). Systematic errors remain in the CMIP6 models, however there are some improvements seen in the spatial simulation of soil carbon from CMIP5. Soil carbon is still underestimated in the northern latitudes, where the areas of blue still remain the northern
330 latitudes of the CMIP6 soil carbon map in Fig. 1(a), though regions of overestimations in the northern latitudes are also seen amongst the CMIP6 models in BCC-CSM2-MR, CESM2, CNRM-ESM2-1, and NorESM2-LM (Fig. 2), but it is noted that this representation might be more consistent with observations if a dataset including deeper soil carbon stocks was considered. CMIP6 shows improvements in the representation of mid-latitude soil carbon, where less of an overestimation is seen in CMIP6 compared with CMIP5 (Fig. 1(a)). This overestimation can still be seen in four of the eleven CMIP6 models: ACCESS-
335 ESM1.5, CanESM2, MIROC-ES2L and UKESM1-0-LL, however the overestimations in CMIP6 are less inconsistent than when compared with CMIP5 and the number of models showing this limitation in CMIP6 has been reduced (Fig. 2).

Despite the differences seen in the spatial representation of soil carbon between the individual models in CMIP6, the ensemble mean has more areas of agreement within the ensemble compared to the ensemble mean in CMIP5. This can be seen in Fig. 3(a), where there is less hatching (where hatched shaded areas represent regions of low agreement amongst the models in the
340 ensemble, see methods) in the CMIP6 map compared with the CMIP5 map. Specifically, ensemble mean soil carbon in CMIP6 has more areas of agreement in the mid-latitude region compared with the CMIP5 ensemble mean, where significant areas of disagreement are seen. This disagreement is likely due to the overestimation which exists in some of the CMIP5 models (Fig. A3). Also, a reduction in the area of disagreement is seen in the northern latitudes in CMIP6 compared with CMIP5, however this remains the region where the most disagreement exists across the generations. It is noted that this is a measure of agree-
345 ment within the ensemble and not between the models and empirical data, so is dependent on choice of ensemble members (see Figures A6 and A7 for individual model maps).

The inconsistency of the simulation of spatial soil carbon in CMIP6 is further evaluated using the spatial standard deviations, the spatial Pearson correlation coefficients and RMSEs (see Methods), where the Taylor Diagram (Fig. 4(a)) presents all three statistical assessments. The spatial standard deviation for soil carbon is shown on the radial axis between standard x and y
350 axes in Fig. 4(a). The range of spatial standard deviations amongst the CMIP6 models sees a slight reduction from the range amongst the CMIP5 models, though significant differences remain. The CMIP6 models CNRM-ESM2-1, MIROC-ES2L and UKESM1-0-LL best match the spatial standard deviation derived from the benchmark dataset (Tables 4 and 5). It is found that the spatial representation of modelled soil carbon in CMIP6 is poorly correlated to the empirical soil carbon, where the

CMIP6 ensemble spatial correlation coefficient with the empirical data is found to be 0.250. The spatial correlation coefficients
355 between the individual CMIP6 and CMIP5 models with the empirical data can also be seen in Fig. 4(a), where the low spatial
correlation coefficients are shown by the curved correlation axis. The lowest spatial correlation coefficients amongst the CMIP6
models were r-values of 0.104 in IPSL-CM6A-LR and 0.115 in UKESM1-0-LL. The CMIP6 model that was the most spatially
consistent with the empirical data is CNRM-ESM2-1, with an r-value of 0.630. The CMIP6 ensemble sees a slight reduction
in the RMSE compared to the CMIP5 ensemble, suggesting a slight improvement (Fig. 5(a)). Significant improvements in the
360 RMSE are seen in MIROC-ES2L from MIROC-ESM and MPI-ESM1.2-LR from MPI-ESM-LR. These results suggest small
improvements in the simulation of soil carbon across this CMIP generation, however the low spatial correlation coefficients
and variable RMSEs seen across the models in CMIP6 suggest inconsistencies with the benchmark data remain.

3.2 Net Primary Productivity: *improved in CMIP6 relative to CMIP5*

3.2.1 Global total evaluation

365 Global total NPP amongst the CMIP6 models appears to be consistent with the benchmark dataset (Table 6), where the CMIP6
ensemble mean for NPP is approximately 95% of the benchmark mean. The CMIP6 ensemble mean global total NPP (53.0
 ± 9.39 PgC yr⁻¹) is found to be slightly lower than the derived mean benchmark value, however it is comfortably within the
observational uncertainty range (56.6 ± 14.3 PgC yr⁻¹). The equivalent values for the CMIP5 models can be seen in Table 7,
where the CMIP5 ensemble total is also found to be within the observational uncertainty range (56.3 ± 15.4 PgC yr⁻¹).

370 The standard deviation surrounding the CMIP5 ensemble mean is greater than in CMIP6. This reduced standard deviation in
CMIP6 is because several of the models have a simulated global total NPP that more closely matches the benchmark NPP global
total value compared with the previous CMIP5 generation. For example, GFDL-ESM4 from GFDL-ESM2G, IPSL-CM6A-LR
from IPSL-CM5A-LR, MIROC-ES2L from MIROC-ESM, MPI-ESM1.2-LR from MPI-ESM1-M, and UKESM1-0-LL from
HadGEM2-ES. The majority of CMIP6 models see a reduction in NPP from the CMIP5 equivalent model, which in general
375 reduces the overestimation of NPP that was seen in the CMIP5 models (Table 7 and 6). However, it was not the case for
CanESM5 from CanESM2 which sees an increase in the magnitude of NPP from CMIP5 to CMIP6, resulting in a consequent
overestimation compared to the benchmark data. A reduced range of modelled global total NPP values is also seen in CMIP6
from CMIP5, where the range is reduced from 48.5 PgC yr⁻¹ in CMIP5 to 32.7 PgC yr⁻¹ in CMIP6. These results suggest
that overall the representation of carbon fluxes in CMIP6 ESMs is more consistent than in CMIP5.

380 3.2.2 Spatial evaluation

Modelled NPP in CMIP6 appears to be spatially more consistent with empirical data than CMIP5. This is suggested by Fig.
1(b), where the difference between the modelled and benchmark NPP is shown for both CMIP5 and CMIP6. It can be seen in
the CMIP5 map that NPP is overestimated in the tropical regions, specifically in Africa and South East Asia, and the equivalent
CMIP6 difference map shows a clear reduction in this overestimation. This tropical overestimation of NPP prominent in CMIP5
385 (Fig. A4), is still seen in the CMIP6 models CanESM5, MPI-ESM1.2-LR and UKESM1-0-LL. However, this is not seen in the

CMIP6 ensemble mean as it is likely negated by underestimations seen in CESM2, CNRM-ESM2-1, and NorESM2-LM (Fig. 6). CMIP6 also sees more consistency with the benchmark dataset in the northern and mid-latitudes compared with CMIP5, where more white areas are seen in the CMIP6 map in Fig. 1(b). An underestimation of NPP is seen in both CMIP5 and CMIP6 on the west side of South America, though unusually high NPP is seen in this region in the MODIS NPP dataset (Fig. A2).
390 Moreover, greater agreement amongst the models within CMIP6 is seen compared the models in CMIP5. This can be seen in Fig. 3(b), where less hatching representing areas of disagreement within the ensemble is seen in the CMIP6 compared with CMIP5. Specifically, CMIP6 sees less hatching in the northern latitudes, the Middle East and South East Europe, as well as regions in South America, South Africa and Australia (see Figures A8 and A9 for individual model maps).

The improved empirical consistency of modelled NPP in CMIP6 is also suggested when further evaluated using the same
395 spatial metrics as with soil carbon. Despite a small range remaining in the spatial standard deviations amongst the CMIP6 models (shown by the radial axis in Fig. 4(b)), robust improvements in the spatial correlation coefficients (shown by the curved axis in Fig. 4(b)) and RMSEs are seen across the ensemble compared with CMIP5 (Fig. 5(b)). Notable improvements in the representation of NPP are seen in GFDL-ESM4 compared with GFDL-ESM2G, IPSL-CM6A-LR compared with IPSL-CM5A-LR, and UKESM1-0-LL compared with HadGEM2-ES, with reduced RMSEs seen in each updated model. A general
400 improvement in the spatial correlation coefficients is seen across all the CMIP6 models, where the circle markers (CMIP6 models) in Fig. 4(b), have higher correlation values than the cross markers (CMIP5 models). The general improvement has resulted in the CMIP6 ensemble correlation coefficient (0.836) being greater compared with the equivalent CMIP5 value (0.711). The lowest correlations between modelled and observed NPP amongst the CMIP5 models are GISS-E2-R (0.274) and CanESM2 (0.469). The updated version CanESM5 remains the lowest correlation seen in CMIP6 (0.655), however an
405 improvement in the correlation is seen. The updated version of the GISS model is not included in the CMIP6 ensemble considered in this study, which could be a reason for the increased ensemble mean correlation. However, this effect does not take away from the improvements seen across the CMIP6 models. HadGEM2-ES (0.764) and MPI-ESM-LR (0.764) were the CMIP5 models with the highest correlation to the benchmark NPP, and the updated CMIP6 equivalents of these models remain the models with the greatest correlations, but again improvements in the correlations are seen (0.816 in UKESM1-0-LL and
410 0.785 MPI-ESM1.2-LR).

3.3 Soil carbon turnover time: *no major improvements in CMIP6 compared to CMIP5*

3.3.1 Global evaluation

There are minor improvements suggested in the simulated effective global τ_s amongst select CMIP6 models (Table 6) compared with CMIP5 (Table 7). The ensemble mean effective global τ_s was overestimated in CMIP5 (37.8 ± 19.7 yr) when compared
415 with the derived mean τ_s using the benchmark datasets (27.0^{+27}_{-11} yr), which is reduced to a less significant underestimation in CMIP6 (23.3 ± 8.59 yr). Though both the CMIP5 and CMIP6 estimates fall within the observational uncertainty range. The associated ensemble spread on effective mean τ_s is less in CMIP6 compared with CMIP5, with a ensemble standard deviation of approximately 50% less. A significant range is seen in the effective global τ_s values amongst the CMIP5 models,

with 5 fold difference between the lowest and the highest values (Table 7). This range is mostly due to large overestimations
420 seen amongst the CMIP5 models, for example in CanESM2, GFDL-ESM2G and MIROC-ESM. A reduced range is seen in
amongst the models in CMIP6, however a 4 fold range still exists between the lowest and the highest values (Table 6). This
reduced range is partly due to reductions in the effective global τ_s values in CMIP6 models compared to the equivalent model
in CMIP5, specifically, CanESM5 from CanESM2, GFDL-ESM4 from GFDL-ESM2G, MIROC-ES2L from MIROC-ESM,
and MPI-ESM1.2-LR from MPI-ESM-LR. Though overestimations do remain in CMIP6, for example in CNRM-ESM2-1,
425 where the slowest effective turnover time was seen. Moreover, the range is also reduced due to improvements seen in models
which underestimated τ_s in CMIP5, such as UKESM1-0-LL from HadGEM2-ES and CESM2 from CCSM4.

3.3.2 Spatial evaluation

The comparison of spatial τ_s in CMIP6 with CMIP5 has more varied results than what was seen in simulated NPP. The CMIP5
ensemble showed an underestimation of τ_s in the northern latitudes, which is replaced with an overestimation of τ_s in CMIP6
430 when compared to the benchmark data (Fig. 1(c)). This northern latitude overestimation in the CMIP6 ensemble is a result of
the overestimations of τ_s in CESM2 and NorESM2-LM (Fig. 7), which dominate in the CMIP6 ensemble mean. It is noted
that this result may differ if deeper soil carbon stocks were considered. The northern latitude underestimation of τ_s is still
seen within the CMIP6 models, such as CanESM5, CNRM-ESM2-1, GFDL-ESM4, IPSL-CM6A-LR, MIROC-ES2L, MPI-
ESM1.2-LR, and UKESM1-0-LL (Fig. 7). An overestimation of mid-latitude τ_s was seen in the CMIP5 models MIROC-ESM
435 and MPI-ESM-LR (Fig. A5), which is no longer seen in the updated CMIP6 models MIROC-ES2L and MPI-ESM1-2-LR.
However, an overestimation of mid-latitude τ_s is seen in CMIP6 models BCC-CSM2-MR, CNRM-ESM2-1 and UKESM1-0-
LL (Fig. 7). The uncertainty in simulated northern latitude τ_s is also apparent in Fig. 3(c), where the hatching shows the lack
of agreement within the CMIP6 ensemble in this region. However, more agreement within the CMIP6 ensemble is seen in the
same figure in the mid-latitudes and tropical regions compared with CMIP5 (see Figures A10 and A11 for individual model
440 maps).

The simulation of spatial τ_s in CMIP6 is further evaluated against the empirical data with the additional statistical metrics.
Modelled τ_s is found to be poorly spatially correlated to empirical τ_s in both the CMIP5 and CMIP6 models (shown by the
curved axis in Fig. 4(c)). A slight increase in the ensemble mean spatial correlations is seen from CMIP5 (0.188) to CMIP6
(0.267), due to increases seen amongst individual models between CMIP5 and CMIP6, such as CESM2 from CCSM4, MPI-
445 ESM1.2-LR from MPI-ESM-LR, and NorESM2-LM from NorESM1-M. However, the consistency of modelled τ_s with the
benchmark datasets remains low. A particularly large range is seen in the spatial standard deviations of τ_s amongst the CMIP6
models, which is an increased range from CMIP5 (shown by the radial axis in Fig. 4(c)). The CMIP6 models with the most
extreme overestimations of the spatial standard deviations compared to the derived benchmark value (NorESM2-LM, CESM2,
and ACCESS-ESM1.5), are also found to have large RMSEs (Fig. 5(c)). Amongst the remaining CMIP6 models, the RMSEs
450 for modelled τ_s remain relatively consistent between CMIP5 and CMIP6.

3.4 Drivers of soil carbon spatial patterns: *Soil carbon spuriously highly correlated with NPP in CMIP5 and CMIP6*

3.4.1 Global drivers

A negligible correlation (≈ 0) is found between the benchmark estimates of soil carbon and NPP, suggesting that soil carbon is not spatially correlated to NPP in the real world. On the other hand, soil carbon and NPP (C_s -NPP) were found to be significantly correlated in the models in both CMIP5 and CMIP6. The C_s -NPP spatial correlation was found to be greater than 0.5 for six out of the ten CMIP5 ESMs and eight out of the eleven models in CMIP6 (Fig. 8(a)). However, a low spatial correlation is found in the CMIP6 models CESM2 (0.134), NorESM2-LM (0.261), and BCC-CSM2-MR (0.214), values most consistent with the benchmark datasets. The C_s - τ_s spatial correlations found in the CMIP6 models tend to underestimate the positive correlation seen in the benchmark datasets (Fig. 8(a)). The majority of CMIP6 models see a negligible or slightly negative C_s - τ_s spatial correlation, despite a low positive correlation produced by the benchmark datasets. The models BCC-CSM2-MR, MIROC-ES2L, and NorESM2-LM are most consistent with the benchmark C_s - τ_s correlation.

The modelled NPP to temperature (NPP-T) spatial correlations in CMIP6 are consistent with the positive relationship seen in the benchmark datasets, however the magnitude of this positive correlation varies amongst the models (Fig. 8(b)). The magnitude of the positive NPP-T correlation is underestimated in CanESM5, GFDL-ESM4, and NorESM2-LM, but otherwise relatively consistent amongst the CMIP6 models. Nonetheless, a much greater range in the modelled NPP-T correlations was seen amongst the CMIP5 models, suggesting an improved representation of this relationship in CMIP6. The variation in modelled NPP- θ correlations remains in CMIP6, with models disagreeing in the sign and magnitude of the correlation of NPP to soil moisture. The modelled NPP- θ correlation is the most consistent with the benchmark correlations in GFDL-ESM4, MPI-ESM1.2-LR and UKESM1-0-LL (Fig. 8(b)).

It is generally agreed across the models in CMIP6 and CMIP5 that τ_s and temperature (T) are negatively correlated, with the exception of MPI-ESM1.2-LR where a slight positive correlation is seen (Fig. 8(c)). This is consistent with the negative τ_s -T correlation derived in the benchmark dataset. There is variation amongst the models in the magnitude of the negative correlation, with a significant overestimation seen in CanESM5. A negative correlation is also seen in the τ_s - θ correlation derived with the benchmark datasets. Inconsistencies with this empirical relationship are seen amongst the models in both CMIP5 and CMIP6, with many negligible and positive correlations deduced (Fig. 8(c)). The exception is again MPI-ESM1.2-LR, which in this case is the model most consistent with the benchmark τ_s - θ correlation.

3.4.2 Regional drivers

The spatial correlations of modelled C_s -NPP are shown to be overestimated at every latitude in both CMIP6 and CMIP5, compared to the equivalent correlations derived from the empirical datasets. It can be seen that the CMIP6 ensemble mean C_s -NPP correlation has an even larger positive bias compared to the benchmark correlation than in CMIP5. The empirical data sees a reduced C_s -NPP correlation in the northern latitudes, whereas a slight but less significant reduction is seen in the models (Fig. 9(a)). The spatial correlation between C_s - τ_s is shown to vary against latitude in the empirical datasets, where a greater correlation is seen in the tropical and northern latitude regions, and a negligible correlation is seen in the mid-latitudes (Fig.

9(b)). The CMIP6 models simulate the negligible $C_s-\tau_s$ seen in the mid-latitudes relatively consistently with the benchmark
485 data, where an improved consistency is seen from CMIP5. However, the CMIP6 models do not simulate the tropical and
northern latitude positive $C_s-\tau_s$ correlations, where a negligible modelled correlation remains in these regions. CMIP5 is more
consistent with the benchmark correlations than in CMIP6, where a positive modelled correlation $C_s-\tau_s$ is seen (Fig. 9(b)).

The spatial correlation between modelled soil carbon and soil moisture ($C_s-\theta$) is consistent with the correlations seen in
the benchmark datasets at every latitude, with an improvement seen in the tropical correlation patterns in CMIP6 compared
490 with CMIP5 (Fig. 9(c)). Both the CMIP5 and CMIP6 ensembles span the benchmark $C_s-\theta$ correlation, though large model
ranges in the $C_s-\theta$ sensitivity are seen across all latitudes. However, there is a reduced ensemble spread in the $C_s-\theta$ correlation
from CMIP5 to CMIP6 in low and mid latitudes. An overestimation of the negative C_s-T correlation seen in the benchmark
datasets is present in both the CMIP5 and CMIP6 models, except the high latitudes (Fig. 9(d)). This modelled C_s-T correlation
is particularly underestimated in the lower tropical latitudes, where a greater positive correlation is seen here in the benchmark
495 datasets. Fig. 9(d) suggests a slight improvement in the modelled tropical C_s-T correlation in CMIP6, and a worsening of
modelled C_s-T in the high latitudes than in CMIP5, when compared to the C_s-T correlations in the benchmark datasets.

4 Discussion

4.1 Soil carbon stocks

4.1.1 Global total soil carbon

500 Simulating global soil carbon stocks that are consistent with empirical data is required to produce reliable projections of
future soil carbon storage and emission (Todd-Brown et al., 2013). This study deduces a CMIP6 ensemble mean global total
soil carbon of 1206 ± 445 PgC (Table 4), using regridded model resolutions (see methods). It is noted that Ito (2011) state
a CMIP6 ensemble of 1553 ± 672 PgC, however the full soil carbon profile is considered for CESM2 and NorESM2-LM,
opposed to a depth of 1m considered in this study. Additionally, this study deduces a CMIP5 equivalent ensemble mean global
505 soil carbon value of 1480 ± 810 PgC (Table 5), using equivalent dates in the historical simulation (1950-2000). Todd-Brown
et al. (2013) state an ensemble mean soil carbon value of 1520 ± 770 PgC in CMIP5, however the Todd-Brown et al. (2013)
study includes the models BCC-CSM1.1, CESM1-CAM5 and INM-CM4, which are missing from the analysis in this study
due to data availability. Anav et al. (2013) present a CMIP5 ensemble mean soil carbon value of 1502 ± 798 PgC, but this
calculation includes multiple model versions (for example, LR and MR) from the same modelling centre in their ensemble.
510 A caveat of this evaluation study is the non-independent nature of CMIP ESMs, where for example CESM2 and NorESM2-
LM share the same Land Surface Model (LSM). Additionally, the ensembles included here do not necessarily represent all
models that exist within each CMIP generation. However, the evaluation completed here allows for general improvements in
the simulation of soil carbon stocks and fluxes between the CMIP5 and CMIP6 generations to be noted, and key areas for
future model development to be highlighted.

515 Despite a suggestion of a reduced spread in model estimates of global total soil carbon within CMIP6 relative to CMIP5, discrepancies remain in the consistency of these estimates with the observations between the two CMIP generations. It should also be noted that CMIP6 does not simply contain updated versions of every model in CMIP5, some new models are included and some CMIP5 models not included in CMIP6. These factors together with the uncertainty associated with empirical datasets has resulted in no robust conclusion being drawn on the improvement of soil carbon simulation in CMIP6 compared to CMIP5.
520 Due to the potential significant feedback that exists between soil carbon and global climate, this lack of consistency reduces our confidence in future projections of climate change (Friedlingstein et al., 2006; Gregory et al., 2009; Arora et al., 2013; Friedlingstein et al., 2014).

4.1.2 Spatial soil carbon patterns

Modelled soil carbon was found to be poorly spatially correlated with the empirical data amongst models in both CMIP5 and
525 CMIP6 (Fig. 4(a)). An improvement in CMIP6 ESMs was seen in the spatial patterns across the mid-latitudes, which were generally overestimated in CMIP5. However, significant underestimations of modelled soil carbon in the northern latitudes still remain, which have a significant impact on model predictions of global total soil carbon stocks (Fig. 1(a)). This systematic underestimation was previously reported in the literature as a limitation of the CMIP5 models, where Todd-Brown et al. (2013) found northern latitude soil carbon to be less consistent with the empirical data than on a global scale. This limitation remains
530 amongst models in the CMIP6 generation, where it was found that the majority of CMIP6 models underestimate northern latitude soil carbon stocks regardless of whether the global soil carbon stocks are underestimated.

However, an exception to this northern latitude underestimation is seen within CMIP6 in the models CESM2 and NorESM2-LM. These ESMs include the LSM CLM5 (Lawrence et al., 2019), which is the first LSM to include the representation of vertically resolved soil carbon in their CMIP simulations. This representation enables the inclusion of separate carbon pools at
535 varying depths in the soil, which aims to more consistently simulate soil carbon with the real world (Koven et al., 2013). This is of particular importance in the northern latitudes, where carbon stocks are expected to exist at much greater depths than the 1m considered in this study (Tarnocai et al., 2009; Ran et al., 2021). This can be seen in Table 3, where increased magnitudes of soil carbon stocks are shown when increased depths are considered using the empirical datasets. A more thorough evaluation of soil carbon in both CESM2 and NorESM2-LM is suggested for future research, with a particular focus on this improved
540 northern latitude soil carbon stocks simulation, however this evaluation of deeper soil carbon stocks (below 1m) is beyond the scope of this study.

Accurately simulating soil carbon in the northern latitude regions is of particular importance as it is a major part of the total global soil carbon pool (Jackson et al., 2017). Additionally, much of the carbon stored in these soil is held within permafrost, which is known to be particularly sensitive to climate change. Permafrost thaw under climate change has the potential to release
545 significant amounts of carbon into the atmosphere over a short period of time with increased warming (Schuur et al., 2015; Zimov et al., 2006; Burke et al., 2017; Hugelius et al., 2020), representing a significant feedback within the climate system. Permafrost dynamics are generally poorly represented in ESMs, where Burke et al. (2020) found CMIP6 ESMs to have a similar representation compared with CMIP5. Underestimating soil carbon in the northern latitudes may result in underestimating the

550 impact of this feedback in future climate change projections. Future improvements are needed to improve the simulation of soil carbon stocks globally, but particularly within the northern latitudes.

4.2 Drivers of soil carbon change

To allow for a more in-depth understanding of the inconsistencies found between modelled and empirical soil carbon, the simulation of above and below ground controls of soil carbon were also evaluated. Simulations of contemporary soil carbon can be disaggregated into the effects of litterfall, which is well approximated by plant Net Primary Productivity (NPP), and effective soil carbon turnover time (τ_s), which is affected by both temperature and moisture of the soil (Koven et al., 2015). 555 If models are to reliably simulate soil carbon in a way that is consistent with empirical data, the spatial drivers of soil carbon, NPP and τ_s , must also be simulated consistently with empirical data. Isolating the effects of NPP and τ_s on soil carbon helps us to break down the simulation of soil carbon to help understand the limitations and inconsistencies seen amongst the models.

4.2.1 NPP

560 An improved simulation of NPP is suggested in the ESMs included from CMIP6, compared with the ESMs from CMIP5. This conclusion is suggested by: an increased number of models in our CMIP6 ensemble have global total NPP values consistent with empirical data (Table 6), the overestimation of tropical NPP amongst CMIP5 models is seen to be reduced amongst the CMIP6 models (Fig. 1(b)), and more agreement is seen within CMIP6 relative to CMIP5 in the simulation of mid and northern latitude NPP (Fig. 3(b)). Modelled NPP was found to be robustly more consistent with the empirical data in our 565 CMIP6 ensemble compared with the CMIP5 ensemble in all statistical evaluation metrics. Since CMIP5, multiple models have seen an addition of a dynamic nitrogen cycle (Davies-Barnard et al., 2020), where the models with nitrogen cycles are highlighted in Fig. 5 by the shaded bars. The results suggest an improvement in the simulation of NPP with the addition of dynamic nitrogen in models. However, CMIP6 models that do not represent a nitrogen cycle also mostly see improvements in the simulation of NPP, suggesting NPP is more constrained by observations in the newest generation of models. CanESM5 is 570 the only ESM within CMIP6 included here to not see an overall improvement in the simulation of NPP, where NPP is found to be overestimated compared with the benchmark dataset. It is likely that the inclusion of a nitrogen cycle in this model would limit this overestimated NPP and improve consistency with the observations (Zhang et al., 2014; Exbrayat et al., 2013).

Despite this apparent improved simulation of NPP in CMIP6, the spatial correlation between modelled soil carbon and NPP was found to be inconsistent with the equivalent empirically derived relationship. This result was previously shown for 575 the CMIP5 models (Todd-Brown et al., 2013), and has been more recently shown for the CMIP6 models (Georgiou et al., 2021), both agreeing with the results found here. The majority of CMIP6 models were found to have positive C_s -NPP spatial correlations, opposed to a negligible spatial correlation found in the observations (Fig. 8(a)). Despite NPP driving the spatial pattern of soil carbon stocks due to carbon input from vegetation, a positive correlation was not expected in the real world due to regions with high soil carbon not correlating with regions of high NPP. For example, in the observational derived data soil 580 carbon stocks are greatest in the northern latitudes due to long turnover times in these regions, whereas NPP is lower due to cold temperatures in these regions limiting vegetation growth. The three CMIP6 models which did not significantly overestimate

this correlation (CESM2, NorESM2-LM, and BCC-CSM2-MR), are three of the models with the most empirically consistent proportion of soil carbon stocks in the northern latitudes. Conversely the tropical regions see high NPP values, but warmer temperatures result in faster turnover times and lower soil carbon stocks. NPP is expected to increase in the future under climate change (Kimball et al., 1993; Friedlingstein et al., 1995; Amthor, 1995), which means an overly positive correlation in models could result in a subsequent increase in modelled projections of soil carbon stocks. An overestimation of future soil carbon storage could result in an overestimation of the future carbon sink and an inaccurate global carbon budget (Todd-Brown et al., 2013; Friedlingstein et al., 2022).

4.2.2 Soil carbon turnover time

The systematic improvements suggested from the evaluation of NPP simulation within our CMIP6 ensemble are not suggested for the simulation of τ_s , where the simulation of τ_s appears to remain inconsistent with the empirical data in CMIP6 from CMIP5. Improvements are suggested within CMIP6 relative to CMIP5, such as more agreement within the ensemble in the mid-latitudes and tropical regions, however less agreement is seen in the northern latitudes (Fig. 3(c)). Northern latitude τ_s is generally underestimated in models, which corresponds to the underestimation of soil carbon seen in these regions. This has been previously identified in ESMs, where it was found that the underestimation of global τ_s amongst the CMIP5 models is primarily due to low values in the northern latitudes (Wu et al., 2018). The reduced agreement in CMIP6 is due to long τ_s values existing in the northern latitudes of CESM2 and NorESM2-LM, alongside the general ensemble underestimations (Fig. 7). The increased northern latitude τ_s values in CESM2 and NorESM2-LM are likely to be due to the representation of vertically resolved soil carbon pools, which allows for differential τ_s values for pools at varying depths. Despite these individual improvements since CMIP5, large discrepancies exist within the CMIP6 ensemble between modelled and empirical τ_s .

To simulate τ_s consistently with observations, the relationship of τ_s to both temperature (T) and moisture (θ) must also be simulated in a way that is consistent with observations. Generally, the τ_s -T relationship is consistently simulated, however there is variation in the modelled temperature sensitivity of τ_s across the ensemble. The τ_s - θ relationship is less consistently represented, where the majority of CMIP6 models do not match the empirically derived relationship. Despite a positive dependence of soil respiration on soil moisture in the empirical data, many of the CMIP6 models display a contradictory positive τ_s - θ correlation (Fig. 8). Many of the models use functions that increase respiration with soil moisture (see Section 2.1) so the increase of τ_s with increasing soil moisture indicated by positive τ_s - θ correlations in the models is unexpected. We note that this effect occurs most strongly in the models with a very strongly negative τ_s -T relationship (Fig. 8(c)), so it could in fact be an artefact of a negative correlation between temperature and soil moisture. In this context it is also important to consider what soil moisture in LSMs represents. The aim within models is to act as the lower boundary condition for atmospheric models, therefore their soil parameters may historically have been tuned to give appropriate evaporation rates and not necessarily to represent the soil moisture itself in an accurate way, so it may be more relevant to consider the large scale emergent patterns of τ_s than the direct relationships between soil moisture and respiration. It is noted that the empirical relationship shows τ_s reducing with higher soil moisture, which suggests that the observations are picking up more on longer turnover times in dry areas

rather than in saturated areas such as peatlands. This may be due to having only surface soil moisture information, whereas peatlands, while saturated at depth, typically have a water table ~ 10 cm below the surface and can be very dry at the surface (Evans et al., 2021). Thus while models do not include the necessary processes for peat formation (Chadburn et al., 2022), this is unlikely to be the cause of the discrepancy since it would lead to even more of a positive τ_s - θ correlation in the models.

620 Different processes control soil carbon formation in different ecosystems, including stabilisation by clay particles, transformation by microbes, nitrogen and phosphorous availability, etc. (Witzgall et al., 2021). In the present study, the largest discrepancies in both soil carbon and turnover times are seen in permafrost and peatland areas (see Fig. 2 and Fig. 7). For example, the west Siberian peatland complex stands out on the majority of the panels in these figures as an area of high model error. This is partly because the soil carbon turnover times and quantities are largest in these regions, but also partly due to
625 the specific controlling processes in these ecosystems. A key part of soil carbon development in permafrost regions is the fact that organic material can be preserved in frozen soil, including via cryoturbation and yedoma deposits, which have not yet been thoroughly represented in models (Beer, 2016; Zhu et al., 2016). There are a variety of other factors, such as plants storing significantly more of their carbon below ground instead of above ground in cold climates, and recalcitrant vegetation such as mosses, which are not represented in most ESMs (Sulman et al., 2021). Peatland formation is controlled primarily
630 by waterlogging, which reduces oxygen available for decomposition, but there are a huge number of additional physical and biogeochemical feedbacks that take place (Waddington et al., 2015). These kinds of small-scale processes and inhomogeneities are difficult to resolve in global models with ~ 100 km² grid cells, and this should be weighed up against their relative impact on global carbon budgets when considering including these processes in ESMs. However, it is suggested that the large-scale discrepancies such as in the permafrost and large peatland areas can and should be resolved in future model versions.

635 Our results suggest much of the uncertainty associated with modelled soil carbon stocks can be attributed to the simulation of below ground processes. The apparent improved consistency of NPP with empirical data suggests considerable efforts have been made to achieve an improved representation of above ground processes in CMIP6 ESMs since the release of the CMIP5 ensemble. However, the same improvements are not apparent in the simulation of τ_s as systemic limitations remain in the new generation of ESMs considered in this study, suggesting the same progress on the model development of below
640 ground processes has not been achieved between CMIP5 and CMIP6. Moreover, focus on above ground processes without consideration of below ground processes can result in inconsistencies of soil carbon stocks. For example, the inclusion of a nitrogen cycle has been shown to lead to a reduction in soil carbon in the model, see Fig. 6 in Wiltshire et al. (2021), so tuning of the baseline turnover rates is required to keep soil carbon stocks consistent with observed values.

The required improvement of soil carbon pool turnover rates has previously been identified for the CMIP5 ensemble (Nishina
645 et al., 2014), and more recently, Ito et al. (2020) find that the difference in turnover times amongst the CMIP6 models is responsible for approximately 88% of the variation seen in global soil carbon stocks amongst the models, and state that constraining key parameters which control soil carbon turnover processes is a key area for future model development. A key development seen in CMIP6 since CMIP5 is the representation of vertically resolved soil carbon. Models which simulate non-vertically resolved soil carbon typically turn over all the carbon based on the temperature near the soil surface. This could lead
650 to reduced quantities of soil carbon and an underestimation of northern latitude soil carbon stocks, due to near surface soil

being warmer than the deeper soil, and as turnover is known to respond exponentially to temperature (Davidson and Janssens, 2006). Overall, further improvements in the representation of soil carbon turnover time, with a particular focus on the northern latitudes, is identified as a key area for future model development.

5 Conclusions

655 The ability of Earth System Models (ESMs) to simulate present day soil carbon is vital to help predict reliable global carbon budget estimates, which are required for Paris agreement targets. In this study, CMIP6 ESMs have been evaluated against empirical datasets to assess their ability to represent soil carbon and related controls: Net Primary Productivity (NPP) and the effective soil carbon turnover time ($\tau_s = C_s/R_h$). The evaluation is completed by comparison to the previous generation of CMIP5 ESMs, to assess where improvements have been made and to identify priorities for future model development. Below
660 the key conclusions from this study are listed:

1. The spatial patterns of soil carbon in CMIP6 models appear to be more in agreement with each other than they were in CMIP5, and are more consistent with observations in the mid-latitudes, although caveats around the uncertainty in observations and the ensemble design make this conclusion uncertain. However, soil carbon is still heavily underestimated in high northern latitudes (with the exception of two CMIP6 models that represent deep soil carbon).
- 665 2. Overall, we are not able to identify significant improvements in the simulation of the observed spatial pattern of soil carbon across the globe from the CMIP5 to the CMIP6 generation.
3. There is good evidence that spatial patterns of contemporary NPP are better simulated in CMIP6 than in CMIP5 generation models, when compared to satellite-derived estimates.
4. However, spatial patterns of τ_s continue to be poorly represented in CMIP6 models, in comparison to estimates derived
670 from observational datasets of soil carbon and heterotrophic respiration (R_h).
5. Importantly, soil carbon simulations in both the CMIP5 and CMIP6 ESM generations seem to be spuriously highly-correlated with NPP, which may make soil carbon in these models over responsive to future projected changes in NPP.

Taken together, these conclusions point to a need for a much greater emphasis on improving the representation of below ground soil processes in next generation (CMIP7) of ESMs.

675 *Data availability.* The datasets analysed during this study are available online: CMIP5 model output [<https://esgf-node.llnl.gov/search/cmip5/>], CMIP6 model output [<https://esgf-node.llnl.gov/search/cmip6/>], Harmonized World Soils Database (HWSD) and Northern Circumpolar Soil Carbon Database (NCSCD) [https://github.com/rebeccamayvarney/CMIP_soilcarbon_evaluation], World Inventory of Soil property Estimates (WISE30sec) [<https://www.isric.org/explore/wise-databases>], Sanderman et al. 2017 soil carbon estimate (1m and 2m) [<https://dataverse.harvard.edu/dataset.xhtml?persistentId=doi:10.7910/DVN/QQQM8V>],

680 Global Soil Dataset for use in Earth System Models (GSDE) [<http://globalchange.bnu.edu.cn/research/soilw>], Global
Gridded Surfaces of Selected Soil Characteristics (IGBP-DIS) [https://daac.ornl.gov/cgi-bin/dsviewer.pl?ds_id=569],
MODIS Net Primary Production [<https://lpdaac.usgs.gov/products/mod17a3v055>], CARDAMOM Heterotrophic
Respiration [<https://datashare.is.ed.ac.uk/handle/10283/875>], Copernicus Climate Change Service (C3S) soil
moisture gridded dataset [<https://cds.climate.copernicus.eu/cdsapp#!/dataset/eu.copernicus.climate.satellite-soil->
685 [moisture?tab=overview&utm_medium=chatbot&utm_source=cds](https://cds.climate.copernicus.eu/cdsapp#!/dataset/eu.copernicus.climate.satellite-soil-moisture?tab=overview&utm_medium=chatbot&utm_source=cds)], and the WFDEI Meteorological Forcing Data
[<https://rda.ucar.edu/datasets/ds314.2/>].

Author contributions. R.M.V., S.E.C., and P.M.C. outlined the evaluation and drafted the manuscript, and R.M.V. completed the analysis and produced the figures. E.J.B. provided the empirical datasets and gave helpful advice to address the empirical uncertainty. All co-authors provided guidance on the study at various times and suggested edits to the draft manuscript.

690 *Competing interests.* The authors declare that they have no competing interests.

Acknowledgements. This work was supported by the European Research Council ‘Emergent Constraints on Climate-Land feedbacks in the Earth System (ECCLES)’ project, grant agreement number 742472 and the European Research Council ‘Climate-Carbon Interactions in the Current Century (4C)’ project, grant agreement number 821003 (R.M.V. and P.M.C.). S.E.C. was supported by a Natural Environment Research Council independent research fellowship, grant no. NE/R015791/1. E.J.B. was supported by the Joint UK BEIS/Defra Met Office
695 Hadley Centre Climate Programme (grant no. GA01101). We acknowledge the World Climate Research Programme’s Working Group on Coupled Modelling, which is responsible for CMIP, and we thank the climate modelling groups for producing and making their model output available to enable studies such as this evaluation study. We also thank providers of empirical datasets, which enabled us to complete the evaluation in this study. The Taylor diagrams presented in this study was produced using code at [<https://gist.github.com/ycopin/3342888>].

References

- 700 Amthor, J. S.: Terrestrial higher-plant response to increasing atmospheric [CO₂] in relation to the global carbon cycle, *Global Change Biology*, 1, 243–274, 1995.
- Anav, A., Friedlingstein, P., Kidston, M., Bopp, L., Ciais, P., Cox, P., Jones, C., Jung, M., Myneni, R., and Zhu, Z.: Evaluating the land and ocean components of the global carbon cycle in the CMIP5 Earth System Models, *Journal of Climate*, 26, 6801–6843, 2013.
- Arora, V. and Boer, G.: Uncertainties in the 20th century carbon budget associated with land use change, *Global Change Biology*, 16, 705 3327–3348, 2010.
- Arora, V., Boer, G., Christian, J., Curry, C., Denman, K., Zahariev, K., Flato, G., Scinocca, J., Merryfield, W., and Lee, W.: The effect of terrestrial photosynthesis down regulation on the twentieth-century carbon budget simulated with the CCCma Earth System Model, *Journal of Climate*, 22, 6066–6088, 2009.
- Arora, V. K., Boer, G. J., Friedlingstein, P., Eby, M., Jones, C. D., Christian, J. R., Bonan, G., Bopp, L., Brovkin, V., Cadule, P., et al.: 710 Carbon–concentration and carbon–climate feedbacks in CMIP5 Earth system models, *Journal of Climate*, 26, 5289–5314, 2013.
- Arora, V. K., Katavouta, A., Williams, R. G., Jones, C. D., Brovkin, V., Friedlingstein, P., Schwinger, J., Bopp, L., Boucher, O., Cadule, P., et al.: Carbon–concentration and carbon–climate feedbacks in CMIP6 models and their comparison to CMIP5 models, *Biogeosciences*, 17, 4173–4222, 2020.
- Batjes, N. H.: Harmonized soil property values for broad-scale modelling (WISE30sec) with estimates of global soil carbon stocks, *Geoderma*, 269, 61–68, 2016. 715
- Beer, C.: Permafrost sub-grid heterogeneity of soil properties key for 3-D soil processes and future climate projections, *Frontiers in Earth Science*, 4, 81, 2016.
- Bentsen, M., Bethke, I., Debernard, J. B., Iversen, T., Kirkevåg, A., Seland, Ø., Drange, H., Roelandt, C., Seierstad, I. A., Hoose, C., et al.: The Norwegian Earth System Model, NorESM1-M–Part 1: description and basic evaluation of the physical climate, *Geoscientific Model Development*, 6, 687–720, 2013. 720
- Best, M., Pryor, M., Clark, D., Rooney, G., Essery, R., Ménard, C., Edwards, J., Hendry, M., Porson, A., Gedney, N., et al.: The Joint UK Land Environment Simulator (JULES), model description–Part 1: energy and water fluxes, *Geoscientific Model Development*, 4, 677–699, 2011.
- Bloom, A., Williams, M., et al.: CARDAMOM 2001-2010 global carbon Model-Data Fusion (MDF) analysis, 2015.
- 725 Boucher, O., Servonnat, J., Albright, A. L., Aumont, O., Balkanski, Y., Bastrikov, V., Bekki, S., Bonnet, R., Bony, S., Bopp, L., et al.: Presentation and evaluation of the IPSL-CM6A-LR climate model, *Journal of Advances in Modeling Earth Systems*, 12, e2019MS002 010, 2020.
- Burke, E. J., Ekici, A., Huang, Y., Chadburn, S. E., Huntingford, C., Ciais, P., Friedlingstein, P., Peng, S., and Krinner, G.: Quantifying uncertainties of permafrost carbon–climate feedbacks, *Biogeosciences*, 14, 3051–3066, 2017.
- 730 Burke, E. J., Zhang, Y., and Krinner, G.: Evaluating permafrost physics in the Coupled Model Intercomparison Project 6 (CMIP6) models and their sensitivity to climate change, *The Cryosphere*, 14, 3155–3174, 2020.
- Canadell, J., Monteiro, P., Costa, M., Cotrim da Cunha, L., Cox, P., Eliseev, A., Henson, S., Ishii, M., Jaccard, S., Koven, C., Lohila, A., Patra, P., Piao, S., Rogelj, J., Syampungani, S., Zaehle, S., and Zickfeld, K.: *Global Carbon and other Biogeochemical Cycles and Feedbacks*, Cambridge University Press, Cambridge, United Kingdom and New York, NY, USA, <https://doi.org/10.1017/9781009157896.007>, 2021.

- 735 Carvalhais, N., Forkel, M., Khomik, M., Bellarby, J., Jung, M., Migliavacca, M., Mu, M., Saatchi, S., Santoro, M., Thurner, M., et al.: Global covariation of carbon turnover times with climate in terrestrial ecosystems, *Nature*, 514, 213, 2014.
- Chadburn, S. E., Burke, E. J., Gallego-Sala, A. V., Smith, N. D., Bret-Harte, M. S., Charman, D. J., Drewer, J., Edgar, C. W., Euskirchen, E. S., Fortuniak, K., et al.: A new approach to simulate peat accumulation, degradation and stability in a global land surface scheme (JULES vn5. 8_accumulate_soil) for northern and temperate peatlands, *Geoscientific Model Development*, 15, 1633–1657, 2022.
- 740 Cheruy, F., Ducharne, A., Hourdin, F., Musat, I., Vignon, É., Gastineau, G., Bastrikov, V., Vuichard, N., Diallo, B., Dufresne, J.-L., et al.: Improved near-surface continental climate in IPSL-CM6A-LR by combined evolutions of atmospheric and land surface physics, *Journal of Advances in Modeling Earth Systems*, 12, e2019MS002 005, 2020.
- Clark, D., Mercado, L., Sitch, S., Jones, C., Gedney, N., Best, M., Pryor, M., Rooney, G., Essery, R., Blyth, E., et al.: The Joint UK Land Environment Simulator (JULES), model description–Part 2: carbon fluxes and vegetation dynamics, *Geoscientific Model Development*, 4, 701–722, 2011.
- 745 Copernicus Climate Change Service, E. K.: Copernicus Climate Change Service, Product User Guide and Specification, https://datastore.copernicus-climate.eu/documents/satellite-soil-moisture/C3S_312b_Lot4.D3.SM.5-v3.0_202101_Product_User_Guide_Specification_i1.0.pdf, 2021.
- Cox, P. M., Betts, R. A., Jones, C. D., Spall, S. A., and Totterdell, I. J.: Acceleration of global warming due to carbon-cycle feedbacks in a coupled climate model, *Nature*, 408, 184, 2000.
- 750 Crowther, T. W., Todd-Brown, K. E., Rowe, C. W., Wieder, W. R., Carey, J. C., Machmuller, M. B., Snoek, B., Fang, S., Zhou, G., Allison, S. D., et al.: Quantifying global soil carbon losses in response to warming, *Nature*, 540, 104, 2016.
- Dai, Y., Zeng, X., Dickinson, R. E., Baker, I., Bonan, G. B., Bosilovich, M. G., Denning, A. S., Dirmeyer, P. A., Houser, P. R., Niu, G., et al.: The common land model, *Bulletin of the American Meteorological Society*, 84, 1013–1024, 2003.
- 755 Danabasoglu, G., Lamarque, J.-F., Bacmeister, J., Bailey, D., DuVivier, A., Edwards, J., Emmons, L., Fasullo, J., Garcia, R., Gettelman, A., et al.: The community earth system model version 2 (CESM2), *Journal of Advances in Modeling Earth Systems*, 12, 2020.
- Davidson, E. A. and Janssens, I. A.: Temperature sensitivity of soil carbon decomposition and feedbacks to climate change, *Nature*, 440, 165, 2006.
- Davies-Barnard, T., Meyerholt, J., Zaehle, S., Friedlingstein, P., Brovkin, V., Fan, Y., Fisher, R. A., Jones, C. D., Lee, H., Peano, D., et al.: Nitrogen cycling in CMIP6 land surface models: progress and limitations, *Biogeosciences*, 17, 5129–5148, 2020.
- 760 Del Grosso, S., Parton, W., Mosier, A., Holland, E., Pendall, E., Schimel, D., and Ojima, D.: Modeling soil CO₂ emissions from ecosystems, *Biogeochemistry*, 73, 71–91, 2005.
- Delire, C., Séférian, R., Decharme, B., Alkama, R., Calvet, J.-C., Carrer, D., Gibelin, A.-L., Joetzjer, E., Morel, X., Rocher, M., et al.: The global land carbon cycle simulated with ISBA-CTRIP: Improvements over the last decade, *Journal of Advances in Modeling Earth Systems*, 12, e2019MS001 886, 2020.
- 765 Dorigo, W., Wagner, W., Albergel, C., Albrecht, F., Balsamo, G., Brocca, L., Chung, D., Ertl, M., Forkel, M., Gruber, A., et al.: ESA CCI Soil Moisture for improved Earth system understanding: State-of-the art and future directions, *Remote Sensing of Environment*, 203, 185–215, 2017.
- Dufresne, J.-L., Foujols, M.-A., Denvil, S., Caubel, A., Marti, O., Aumont, O., Balkanski, Y., Bekki, S., Bellenger, H., Benshila, R., et al.: Climate change projections using the IPSL-CM5 Earth System Model: from CMIP3 to CMIP5, *Climate dynamics*, 40, 2123–2165, 2013.
- 770

- Dunne, J., Horowitz, L., Adcroft, A., Ginoux, P., Held, I., John, J., Krasting, J., Malyshev, S., Naik, V., Paulot, F., et al.: The GFDL Earth System Model version 4.1 (GFDL-ESM 4.1): Overall coupled model description and simulation characteristics, *Journal of Advances in Modeling Earth Systems*, 12, e2019MS002015, 2020.
- 775 Dunne, J. P., John, J. G., Adcroft, A. J., Griffies, S. M., Hallberg, R. W., Shevliakova, E., Stouffer, R. J., Cooke, W., Dunne, K. A., Harrison, M. J., et al.: GFDL's ESM2 global coupled climate-carbon earth system models. Part I: Physical formulation and baseline simulation characteristics, *Journal of climate*, 25, 6646–6665, 2012.
- Dunne, J. P., John, J. G., Shevliakova, E., Stouffer, R. J., Krasting, J. P., Malyshev, S. L., Milly, P., Sentman, L. T., Adcroft, A. J., Cooke, W., et al.: GFDL's ESM2 global coupled climate-carbon earth system models. Part II: carbon system formulation and baseline simulation characteristics, *Journal of Climate*, 26, 2247–2267, 2013.
- 780 Eswaran, H., Van Den Berg, E., and Reich, P.: Organic carbon in soils of the world, *Soil science society of America journal*, 57, 192–194, 1993.
- Evans, C., Peacock, M., Baird, A., Artz, R., Burden, A., Callaghan, N., Chapman, P., Cooper, H., Coyle, M., Craig, E., et al.: Overriding water table control on managed peatland greenhouse gas emissions, *Nature*, 593, 548–552, 2021.
- Exbrayat, J.-F., Pitman, A., Zhang, Q., Abramowitz, G., and Wang, Y.-P.: Examining soil carbon uncertainty in a global model: response of 785 microbial decomposition to temperature, moisture and nutrient limitation, *Biogeosciences*, 10, 7095–7108, 2013.
- Eyring, V., Bony, S., Meehl, G. A., Senior, C. A., Stevens, B., Stouffer, R. J., and Taylor, K. E.: Overview of the Coupled Model Intercomparison Project Phase 6 (CMIP6) experimental design and organization, *Geoscientific Model Development (Online)*, 9, 2016.
- FAO, I. and ISRIC, I.: JRC: Harmonized World Soil Database (version 1.2), FAO, Rome, Italy and IIASA, Laxenburg, Austria, 2012.
- Friedlingstein, P., Fung, I., Holland, E., John, J., Brasseur, G., Erickson, D., and Schimel, D.: On the contribution of CO₂ fertilization to the 790 missing biospheric sink, *Global Biogeochemical Cycles*, 9, 541–556, 1995.
- Friedlingstein, P., Cox, P., Betts, R., Bopp, L., von Bloh, W., Brovkin, V., Cadule, P., Doney, S., Eby, M., Fung, I., et al.: Climate-carbon cycle feedback analysis: results from the C4MIP model intercomparison, *Journal of climate*, 19, 3337–3353, 2006.
- Friedlingstein, P., Meinshausen, M., Arora, V. K., Jones, C. D., Anav, A., Liddicoat, S. K., and Knutti, R.: Uncertainties in CMIP5 climate projections due to carbon cycle feedbacks, *Journal of Climate*, 27, 511–526, 2014.
- 795 Friedlingstein, P., Jones, M. W., O'Sullivan, M., Andrew, R. M., Bakker, D. C., Hauck, J., Le Quéré, C., Peters, G. P., Peters, W., Pongratz, J., et al.: Global carbon budget 2021, *Earth System Science Data*, 14, 1917–2005, 2022.
- Gent, P. R., Danabasoglu, G., Donner, L. J., Holland, M. M., Hunke, E. C., Jayne, S. R., Lawrence, D. M., Neale, R. B., Rasch, P. J., Vertenstein, M., et al.: The community climate system model version 4, *Journal of climate*, 24, 4973–4991, 2011.
- Georgiou, K., Malhotra, A., Wieder, W. R., Ennis, J. H., Hartman, M. D., Sulman, B. N., Berhe, A. A., Grandy, A. S., Kyker-Snowman, E., 800 Lajtha, K., et al.: Divergent controls of soil organic carbon between observations and process-based models, *Biogeochemistry*, 156, 5–17, 2021.
- Goll, D. S., Brovkin, V., Liski, J., Raddatz, T., Thum, T., and Todd-Brown, K. E.: Strong dependence of CO₂ emissions from anthropogenic land cover change on initial land cover and soil carbon parametrization, *Global Biogeochemical Cycles*, 29, 1511–1523, 2015.
- Goll, D. S., Winkler, A. J., Raddatz, T., Dong, N., Prentice, I. C., Ciais, P., and Brovkin, V.: Carbon-nitrogen interactions in idealized 805 simulations with JSBACH (version 3.10), *Geoscientific Model Development*, 10, 2009–2030, 2017.
- Gregory, J. M., Jones, C., Cadule, P., and Friedlingstein, P.: Quantifying carbon cycle feedbacks, *Journal of Climate*, 22, 5232–5250, 2009.
- Gruber, A., Dorigo, W. A., Crow, W., and Wagner, W.: Triple collocation-based merging of satellite soil moisture retrievals, *IEEE Transactions on Geoscience and Remote Sensing*, 55, 6780–6792, 2017.

- Guimberteau, M., Zhu, D., Maignan, F., Huang, Y., Yue, C., Dantec-Nédélec, S., Ottlé, C., Jornet-Puig, A., Bastos, A., Laurent, P., et al.: ORCHIDEE-MICT (v8. 4.1), a land surface model for the high latitudes: model description and validation, *Geoscientific Model Development*, 11, 121–163, 2018.
- Hajima, T., Watanabe, M., Yamamoto, A., Tatebe, H., Noguchi, M. A., Abe, M., Ohgaito, R., Ito, A., Yamazaki, D., Okajima, H., et al.: Development of the MIROC-ES2L Earth system model and the evaluation of biogeochemical processes and feedbacks, *Geoscientific Model Development*, 13, 2197–2244, 2020.
- 815 Harper, A. B., Wiltshire, A. J., Cox, P. M., Friedlingstein, P., Jones, C. D., Mercado, L. M., Sitch, S., Williams, K., and Duran-Rojas, C.: Vegetation distribution and terrestrial carbon cycle in a carbon cycle configuration of JULES4. 6 with new plant functional types, *Geoscientific Model Development*, 11, 2857–2873, 2018.
- Haverd, V., Smith, B., Nieradzik, L., Briggs, P. R., Woodgate, W., Trudinger, C. M., Canadell, J. G., and Cuntz, M.: A new version of the CABLE land surface model (Subversion revision r4601) incorporating land use and land cover change, woody vegetation demography, and a novel optimisation-based approach to plant coordination of photosynthesis, *Geoscientific Model Development*, 11, 2995–3026, 2018.
- 820 Hugelius, G., Tarnocai, C., Broll, G., Canadell, J., Kuhry, P., and Swanson, D.: The Northern Circumpolar Soil Carbon Database: spatially distributed datasets of soil coverage and soil carbon storage in the northern permafrost regions, *Earth System Science Data*, 5, 3–13, 2013.
- Hugelius, G., Loisel, J., Chadburn, S., Jackson, R. B., Jones, M., MacDonald, G., Marushchak, M., Olefeldt, D., Packalen, M., Siewert, M. B., et al.: Large stocks of peatland carbon and nitrogen are vulnerable to permafrost thaw, *Proceedings of the National Academy of Sciences*, 117, 20438–20446, 2020.
- 825 IGBP: Global Gridded Surfaces of Selected Soil Characteristics (IGBP-DIS).[Global Gridded Surfaces of Selected Soil Characteristics (International Geosphere-Biosphere Programme-Data and Information System)], <https://doi.org/10.3334/ORNLDAAC/569>, 2000.
- IPCC: Climate Change 2021: The Physical Science Basis. Contribution of Working Group I to the Sixth Assessment Report of the Intergovernmental Panel on Climate Change, vol. In Press, Cambridge University Press, Cambridge, United Kingdom and New York, NY, USA, <https://doi.org/10.1017/9781009157896>, 2021.
- 830 Ito, A.: A historical meta-analysis of global terrestrial net primary productivity: are estimates converging?, *Global Change Biology*, 17, 3161–3175, 2011.
- Ito, A. and Oikawa, T.: A simulation model of the carbon cycle in land ecosystems (Sim-CYCLE): a description based on dry-matter production theory and plot-scale validation, *Ecological Modelling*, 151, 143–176, 2002.
- 835 Ito, A., Hajima, T., Lawrence, D. M., Brovkin, V., Delire, C., Guenet, B., Jones, C. D., Malyshev, S., Materia, S., McDermid, S. P., et al.: Soil carbon sequestration simulated in CMIP6-LUMIP models: implications for climatic mitigation, *Environmental Research Letters*, 15, 124061, 2020.
- Iversen, T., Bentsen, M., Bethke, I., Debernard, J., Kirkevåg, A., Seland, Ø., Drange, H., Kristjansson, J., Medhaug, I., Sand, M., et al.: The Norwegian earth system model, NorESM1-M–Part 2: climate response and scenario projections, *Geoscientific Model Development*, 6, 389–415, 2013.
- 840 Jackson, R. B., Lajtha, K., Crow, S. E., Hugelius, G., Kramer, M. G., and Piñeiro, G.: The ecology of soil carbon: pools, vulnerabilities, and biotic and abiotic controls, *Annual Review of Ecology, Evolution, and Systematics*, 48, 419–445, 2017.
- Ji, D., Wang, L., Feng, J., Wu, Q., Cheng, H., Zhang, Q., Yang, J., Dong, W., Dai, Y., Gong, D., et al.: Description and basic evaluation of Beijing Normal University Earth system model (BNU-ESM) version 1, *Geoscientific Model Development*, 7, 2039–2064, 2014.
- 845 Ji, J., Huang, M., and Li, K.: Prediction of carbon exchanges between China terrestrial ecosystem and atmosphere in 21st century, *Science in China Series D: Earth Sciences*, 51, 885–898, 2008.

- Jobbágy, E. G. and Jackson, R. B.: The vertical distribution of soil organic carbon and its relation to climate and vegetation, *Ecological applications*, 10, 423–436, 2000.
- Jones, C., Hughes, J., Bellouin, N., Hardiman, S., Jones, G., Knight, J., Liddicoat, S., O’connor, F., Andres, R. J., Bell, C., et al.: The
850 HadGEM2-ES implementation of CMIP5 centennial simulations, *Geoscientific Model Development*, 4, 543–570, 2011.
- Kimball, B., Mauney, J., Nakayama, F., and Idso, S.: Effects of increasing atmospheric CO₂ on vegetation, *Vegetatio*, 104, 65–75, 1993.
- Knorr, W.: Annual and interannual CO₂ exchanges of the terrestrial biosphere: Process-based simulations and uncertainties, *Global Ecology and Biogeography*, 9, 225–252, 2000.
- Koven, C., Riley, W., Subin, Z., Tang, J., Torn, M., Collins, W., Bonan, G., Lawrence, D., and Swenson, S.: The effect of vertically resolved
855 soil biogeochemistry and alternate soil C and N models on C dynamics of CLM4, *Biogeosciences*, 10, 7109–7131, 2013.
- Koven, C. D., Chambers, J. Q., Georgiou, K., Knox, R., Negron-Juarez, R., Riley, W. J., Arora, V. K., Brovkin, V., Friedlingstein, P., and Jones, C. D.: Controls on terrestrial carbon feedbacks by productivity versus turnover in the CMIP5 Earth System Models, *Biogeosciences*, 12, 5211–5228, <https://doi.org/10.5194/bg-12-5211-2015>, 2015.
- Koven, C. D., Hugelius, G., Lawrence, D. M., and Wieder, W. R.: Higher climatological temperature sensitivity of soil carbon in cold than
860 warm climates, *Nature Climate Change*, 7, 817, 2017.
- Krinner, G., Viovy, N., de Noblet-Ducoudré, N., Ogée, J., Polcher, J., Friedlingstein, P., Ciais, P., Sitch, S., and Prentice, I. C.: A dynamic global vegetation model for studies of the coupled atmosphere-biosphere system, *Global Biogeochemical Cycles*, 19, 2005.
- Lawrence, D. M., Oleson, K. W., Flanner, M. G., Thornton, P. E., Swenson, S. C., Lawrence, P. J., Zeng, X., Yang, Z.-L., Levis, S., Sakaguchi, K., et al.: Parameterization improvements and functional and structural advances in version 4 of the Community Land Model, *Journal of*
865 *Advances in Modeling Earth Systems*, 3, 2011.
- Lawrence, D. M., Fisher, R. A., Koven, C. D., Oleson, K. W., Swenson, S. C., Bonan, G., Collier, N., Ghimire, B., Van Kampenhout, L., Kennedy, D., et al.: The Community Land Model version 5: Description of new features, benchmarking, and impact of forcing uncertainty, *Journal of Advances in Modeling Earth Systems*, 11, 4245–4287, 2019.
- Liu, Y., Dorigo, W. A., Parinussa, R., de Jeu, R. A., Wagner, W., McCabe, M. F., Evans, J., and Van Dijk, A.: Trend-preserving blending of
870 passive and active microwave soil moisture retrievals, *Remote Sensing of Environment*, 123, 280–297, 2012.
- Liu, Y. Y., Parinussa, R., Dorigo, W. A., De Jeu, R. A., Wagner, W., Van Dijk, A., McCabe, M. F., and Evans, J.: Developing an improved soil moisture dataset by blending passive and active microwave satellite-based retrievals, *Hydrology and Earth System Sciences*, 15, 425–436, 2011.
- Lloyd, J. and Taylor, J.: On the temperature dependence of soil respiration, *Functional ecology*, pp. 315–323, 1994.
- 875 Mauritsen, T., Bader, J., Becker, T., Behrens, J., Bittner, M., Brokopf, R., Brovkin, V., Claussen, M., Crueger, T., Esch, M., et al.: Developments in the MPI-M Earth System Model version 1.2 (MPI-ESM1. 2) and its response to increasing CO₂, *Journal of Advances in Modeling Earth Systems*, 11, 998–1038, 2019.
- Meehl, G. A., Boer, G. J., Covey, C., Latif, M., and Stouffer, R. J.: The coupled model intercomparison project (CMIP), *Bulletin of the American Meteorological Society*, 81, 313–318, 2000.
- 880 Meehl, G. A., Moss, R., Taylor, K. E., Eyring, V., Stouffer, R. J., Bony, S., and Stevens, B.: Climate model intercomparisons: Preparing for the next phase, *Eos, Transactions American Geophysical Union*, 95, 77–78, 2014.
- Melton, J. R., Arora, V. K., Wisernig-Cojoc, E., Seiler, C., Fortier, M., Chan, E., and Teckentrup, L.: CLASSIC v1. 0: the open-source community successor to the Canadian Land Surface Scheme (CLASS) and the Canadian Terrestrial Ecosystem Model (CTEM)–Part 1: Model framework and site-level performance, *Geoscientific Model Development*, 13, 2825–2850, 2020.

- 885 Met Office: Iris: A Python package for analysing and visualising meteorological and oceanographic data sets, Exeter, Devon, v1.2 edn.,
<http://scitools.org.uk/>, 2010 - 2013.
- Nishina, K., Ito, A., Beerling, D., Cadule, P., Ciais, P., Clark, D., Falloon, P., Friend, A., Kahana, R., Kato, E., et al.: Quantifying uncertainties
in soil carbon responses to changes in global mean temperature and precipitation, *Earth System Dynamics*, 5, 197–209, 2014.
- Pan, Y., Birdsey, R. A., Fang, J., Houghton, R., Kauppi, P. E., Kurz, W. A., Phillips, O. L., Shvidenko, A., Lewis, S. L., Canadell, J. G., et al.:
890 A large and persistent carbon sink in the world's forests, *Science*, 333, 988–993, 2011.
- Post, W. M., Emanuel, W. R., Zinke, P. J., and Stangenberger, A. G.: Soil carbon pools and world life zones, *Nature*, 298, 156–159, 1982.
- Raddatz, T., Reick, C., Knorr, W., Kattge, J., Roeckner, E., Schnur, R., Schnitzler, K.-G., Wetzel, P., and Jungclaus, J.: Will the tropical land
biosphere dominate the climate–carbon cycle feedback during the twenty-first century?, *Climate dynamics*, 29, 565–574, 2007.
- Raich, J. W. and Schlesinger, W. H.: The global carbon dioxide flux in soil respiration and its relationship to vegetation and climate, *Tellus*
895 B, 44, 81–99, 1992.
- Ran, Y., Li, X., Cheng, G., Che, J., Aalto, J., Karjalainen, O., Hjort, J., Luoto, M., Jin, H., Obu, J., et al.: New high-resolution estimates of the
permafrost thermal state and hydrothermal conditions over the Northern Hemisphere, *Earth System Science Data Discussions*, pp. 1–27,
2021.
- Sanderman, J., Hengl, T., and Fiske, G. J.: Soil carbon debt of 12,000 years of human land use, *Proceedings of the National Academy of*
900 *Sciences*, 114, 9575–9580, 2017.
- Sato, H., Itoh, A., and Kohyama, T.: SEIB–DGVM: A new Dynamic Global Vegetation Model using a spatially explicit individual-based
approach, *Ecological Modelling*, 200, 279–307, 2007.
- Schmidt, G. A., Kelley, M., Nazarenko, L., Ruedy, R., Russell, G. L., Aleinov, I., Bauer, M., Bauer, S. E., Bhat, M. K., Bleck, R., et al.:
Configuration and assessment of the GISS ModelE2 contributions to the CMIP5 archive, *Journal of Advances in Modeling Earth Systems*,
905 6, 141–184, 2014.
- Schuur, E. A., McGuire, A. D., Schädel, C., Grosse, G., Harden, J. W., Hayes, D. J., Hugelius, G., Koven, C. D., Kuhry, P., Lawrence, D. M.,
et al.: Climate change and the permafrost carbon feedback, *Nature*, 520, 171–179, 2015.
- Séférian, R., Nabat, P., Michou, M., Saint-Martin, D., Voltaire, A., Colin, J., Decharme, B., Delire, C., Berthet, S., Chevallier, M., et al.:
Evaluation of CNRM earth system model, CNRM-ESM2-1: Role of earth system processes in present-day and future climate, *Journal of*
910 *Advances in Modeling Earth Systems*, 11, 4182–4227, 2019.
- Seiler, C., Melton, J. R., Arora, V. K., and Wang, L.: CLASSIC v1. 0: the open-source community successor to the Canadian Land Surface
Scheme (CLASS) and the Canadian Terrestrial Ecosystem Model (CTEM)—Part 2: Global benchmarking, *Geoscientific Model Develop-*
ment, 14, 2371–2417, 2021.
- Seland, Ø., Bentsen, M., Olivie, D., Toniazzo, T., Gjermundsen, A., Graff, L. S., Debernard, J. B., Gupta, A. K., He, Y.-C., Kirkevåg, A.,
915 et al.: Overview of the Norwegian Earth System Model (NorESM2) and key climate response of CMIP6 DECK, historical, and scenario
simulations, *Geoscientific Model Development*, 13, 6165–6200, 2020.
- Sellar, A. A., Walton, J., Jones, C. G., Wood, R., Abraham, N. L., Andrejczuk, M., Andrews, M. B., Andrews, T., Archibald, A. T., de Mora,
L., et al.: Implementation of UK Earth system models for CMIP6, *Journal of Advances in Modeling Earth Systems*, 12, e2019MS001 946,
2020.
- 920 Shangguan, W., Dai, Y., Duan, Q., Liu, B., and Yuan, H.: A global soil data set for earth system modeling, *Journal of Advances in Modeling*
Earth Systems, 6, 249–263, 2014.

- Shevliakova, E., Pacala, S. W., Malyshev, S., Hurtt, G. C., Milly, P., Caspersen, J. P., Sentman, L. T., Fisk, J. P., Wirth, C., and Crevoisier, C.: Carbon cycling under 300 years of land use change: Importance of the secondary vegetation sink, *Global Biogeochemical Cycles*, 23, 2009.
- 925 Sombroek, W. G., Nachtergaele, F. O., and Hebel, A.: Amounts, dynamics and sequestering of carbon in tropical and subtropical soils, *Ambio (Journal of the Human Environment, Research and Management)*;(Sweden), 22, 1993.
- Song, X., Wang, D.-Y., Li, F., and Zeng, X.-D.: Evaluating the performance of CMIP6 Earth system models in simulating global vegetation structure and distribution, *Advances in Climate Change Research*, 12, 584–595, 2021.
- Sulman, B. N., Salmon, V. G., Iversen, C. M., Breen, A. L., Yuan, F., and Thornton, P. E.: Integrating Arctic Plant Functional Types
930 in a Land Surface Model Using Above-and Belowground Field Observations, *Journal of Advances in Modeling Earth Systems*, 13, e2020MS002396, 2021.
- Swart, N. C., Cole, J. N., Kharin, V. V., Lazare, M., Scinocca, J. F., Gillett, N. P., Anstey, J., Arora, V., Christian, J. R., Hanna, S., et al.: The Canadian earth system model version 5 (CanESM5. 0.3), *Geoscientific Model Development*, 12, 4823–4873, 2019.
- Tarnocai, C., Canadell, J., Schuur, E. A., Kuhry, P., Mazhitova, G., and Zimov, S.: Soil organic carbon pools in the northern circumpolar
935 permafrost region, *Global biogeochemical cycles*, 23, 2009.
- Taylor, K. E.: Summarizing multiple aspects of model performance in a single diagram, *Journal of Geophysical Research: Atmospheres*, 106, 7183–7192, 2001.
- Taylor, K. E., Stouffer, R. J., and Meehl, G. A.: An overview of CMIP5 and the experiment design, *Bulletin of the American Meteorological Society*, 93, 485–498, 2012.
- 940 Todd-Brown, K., Randerson, J., Post, W., Hoffman, F., Tarnocai, C., Schuur, E., and Allison, S.: Causes of variation in soil carbon simulations from CMIP5 Earth system models and comparison with observations, *Biogeosciences*, 10, 1717–1736, 2013.
- Trudinger, C. M., Haverd, V., Briggs, P. R., and Canadell, J. G.: Interannual variability in Australia’s terrestrial carbon cycle constrained by multiple observation types, *Biogeosciences*, 13, 6363–6383, 2016.
- UNFCCC: Adoption of The Paris Agreement [UNFCCC/CP/2015/L.9/Rev.1](http://unfccc.int/resource/docs/2015/cop21/eng/l09r01.pdf), <http://unfccc.int/resource/docs/2015/cop21/eng/l09r01.pdf>, 2015.
- 945 Varney, R. M., Chadburn, S. E., Friedlingstein, P., Burke, E. J., Koven, C. D., Hugelius, G., and Cox, P. M.: A spatial emergent constraint on the sensitivity of soil carbon turnover to global warming, *Nature communications*, 11, 1–8, 2020.
- Waddington, J., Morris, P., Kettridge, N., Granath, G., Thompson, D., and Moore, P.: Hydrological feedbacks in northern peatlands, *Ecohydrology*, 8, 113–127, 2015.
- Wagner, W., Dorigo, W., de Jeu, R., Fernandez, D., Benveniste, J., Haas, E., Ertl, M., et al.: Fusion of active and passive microwave obser-
950 vations to create an essential climate variable data record on soil moisture, *ISPRS Annals of the Photogrammetry, Remote Sensing and Spatial Information Sciences (ISPRS Annals)*, 7, 315–321, 2012.
- Watanabe, S., Hajima, T., Sudo, K., Nagashima, T., Takemura, T., Okajima, H., Nozawa, T., Kawase, H., Abe, M., Yokohata, T., et al.: MIROC-ESM 2010: Model description and basic results of CMIP5-20c3m experiments, *Geoscientific Model Development*, 4, 845–872, 2011.
- 955 Weedon, G. P., Balsamo, G., Bellouin, N., Gomes, S., Best, M. J., and Viterbo, P.: The WFDEI meteorological forcing data set: WATCH Forcing Data methodology applied to ERA-Interim reanalysis data, *Water Resources Research*, 50, 7505–7514, 2014.
- Wiltshire, A. J., Burke, E. J., Chadburn, S. E., Jones, C. D., Cox, P. M., Davies-Barnard, T., Friedlingstein, P., Harper, A. B., Liddicoat, S., Sitch, S., et al.: JULES-CN: a coupled terrestrial carbon–nitrogen scheme (JULES vn5. 1), *Geoscientific Model Development*, 14, 2161–2186, 2021.

- 960 Witzgall, K., Vidal, A., Schubert, D. I., Höschen, C., Schweizer, S. A., Buegger, F., Pouteau, V., Chenu, C., and Mueller, C. W.: Particulate organic matter as a functional soil component for persistent soil organic carbon, *Nature communications*, 12, 1–10, 2021.
- Wu, D., Piao, S., Liu, Y., Ciais, P., and Yao, Y.: Evaluation of CMIP5 earth system models for the spatial patterns of biomass and soil carbon turnover times and their linkage with climate, *Journal of Climate*, 31, 5947–5960, 2018.
- Wu, T., Lu, Y., Fang, Y., Xin, X., Li, L., Li, W., Jie, W., Zhang, J., Liu, Y., Zhang, L., et al.: The Beijing Climate Center climate system model
965 (BCC-CSM): The main progress from CMIP5 to CMIP6, *Geoscientific Model Development*, 12, 1573–1600, 2019.
- Yue, X. and Unger, N.: The Yale Interactive terrestrial Biosphere model version 1.0: description, evaluation and implementation into NASA GISS ModelE2, *Geoscientific Model Development*, 8, 2399–2417, 2015.
- Zhang, Q., Wang, Y.-P., Matear, R., Pitman, A., and Dai, Y.: Nitrogen and phosphorous limitations significantly reduce future allowable CO₂ emissions, *Geophysical Research Letters*, 41, 632–637, 2014.
- 970 Zhao, M., Heinsch, F. A., Nemani, R. R., and Running, S. W.: Improvements of the MODIS terrestrial gross and net primary production global data set, *Remote sensing of Environment*, 95, 164–176, 2005.
- Zhao, M., Golaz, J.-C., Held, I., Guo, H., Balaji, V., Benson, R., Chen, J.-H., Chen, X., Donner, L., Dunne, J., et al.: The GFDL global atmosphere and land model AM4. 0/LM4. 0: 2. Model description, sensitivity studies, and tuning strategies, *Journal of Advances in Modeling Earth Systems*, 10, 735–769, 2018.
- 975 Zhu, D., Peng, S., Ciais, P., Zech, R., Krinner, G., Zimov, S., and Grosse, G.: Simulating soil organic carbon in yedoma deposits during the Last Glacial Maximum in a land surface model, *Geophysical Research Letters*, 43, 5133–5142, 2016.
- Ziehn, T., Chamberlain, M. A., Law, R. M., Lenton, A., Bodman, R. W., Dix, M., Stevens, L., Wang, Y.-P., and Srbinovsky, J.: The Australian Earth System Model: ACCESS-ESM1. 5, *Journal of Southern Hemisphere Earth Systems Science*, 70, 193–214, 2020.
- Zimov, S. A., Schuur, E. A., and Chapin III, F. S.: Permafrost and the global carbon budget, *Science(Washington)*, 312, 1612–1613, 2006.

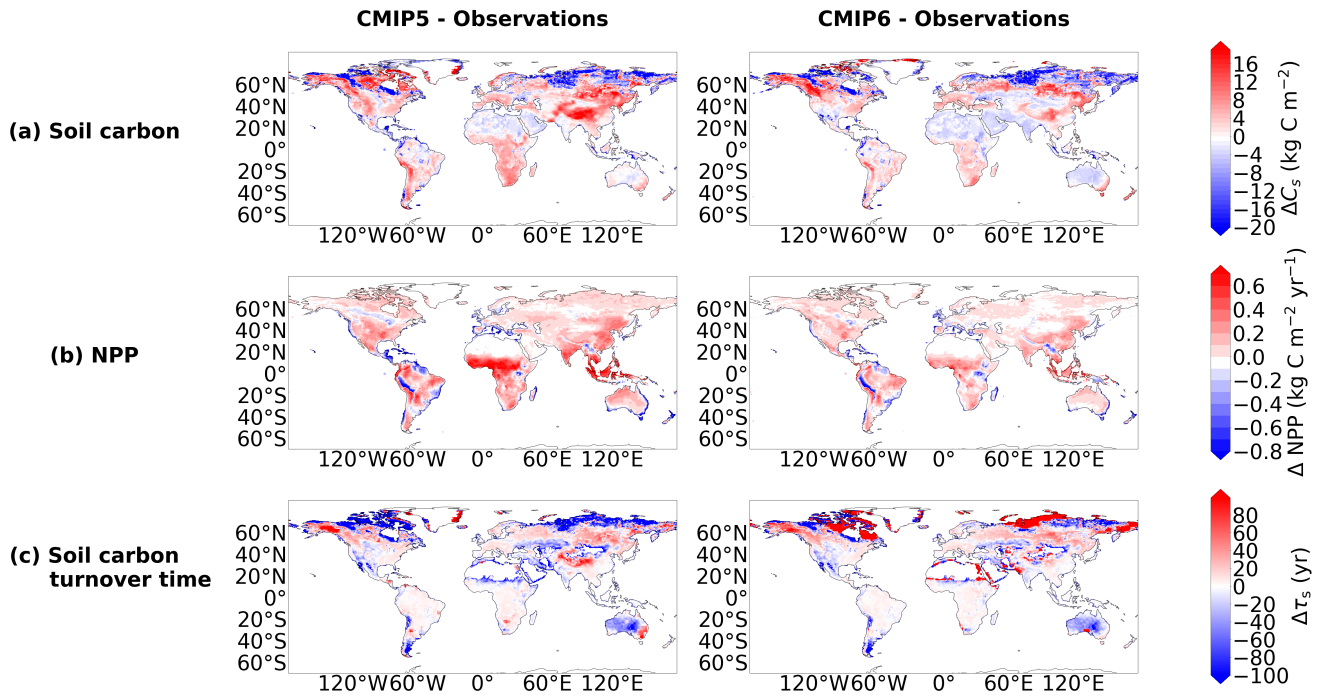


Figure 1. Maps presenting the difference between the modelled and benchmark data for the CMIP5 and CMIP6 ensembles, for: (a) C_s (kg m⁻²), (b) NPP (kg m⁻² yr⁻¹), and (c) τ_s (yr).

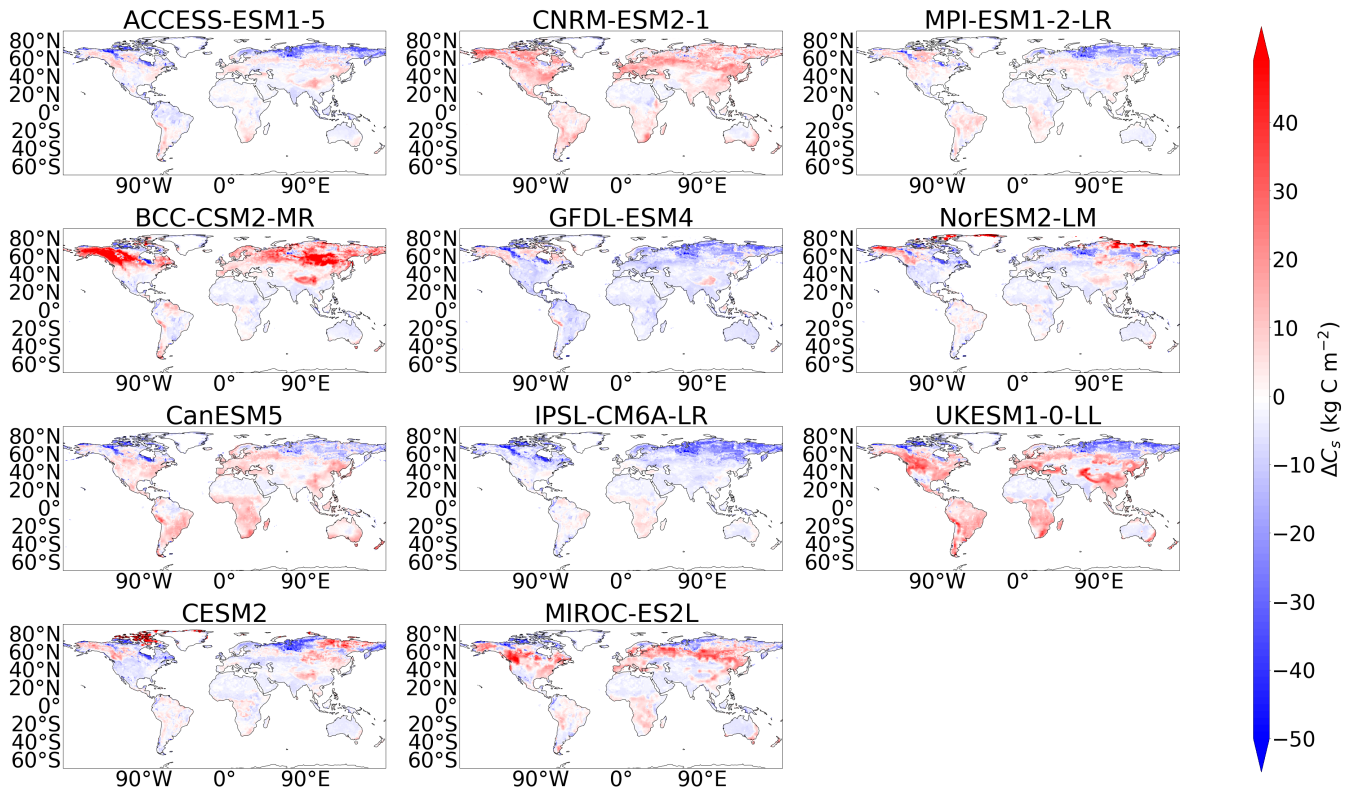


Figure 2. Maps of the difference in soil carbon (C_s) between the historical simulation of each CMIP6 model and the benchmark data.

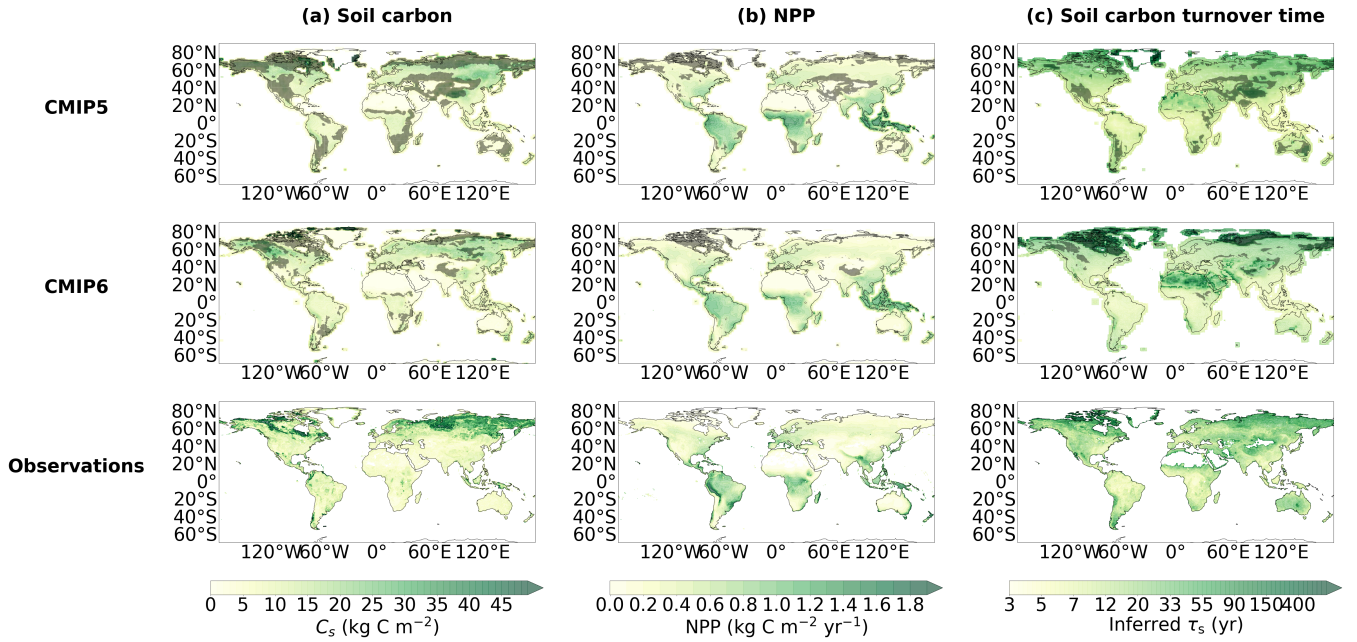


Figure 3. Ensemble mean maps for (a) C_s (kg m^{-2}), (b) NPP ($\text{kg m}^{-2} \text{ yr}^{-1}$), and (c) τ_s (yr), presented for the CMIP6 ensemble, CMIP5 ensemble and the benchmark datasets. The hatched areas are used to show regions of low agreement within the ensemble ($std/mean > 0.75$), and where regions of low soil carbon ($< 5 \text{ kg m}^{-2}$) have been excluded. Equivalent maps for the individual CMIP6 and CMIP5 models are shown within the Appendix, see Figures A6 and A7 for C_s , Figures A8 and A9 for NPP and Figures A10 and A11 for τ_s , respectively.

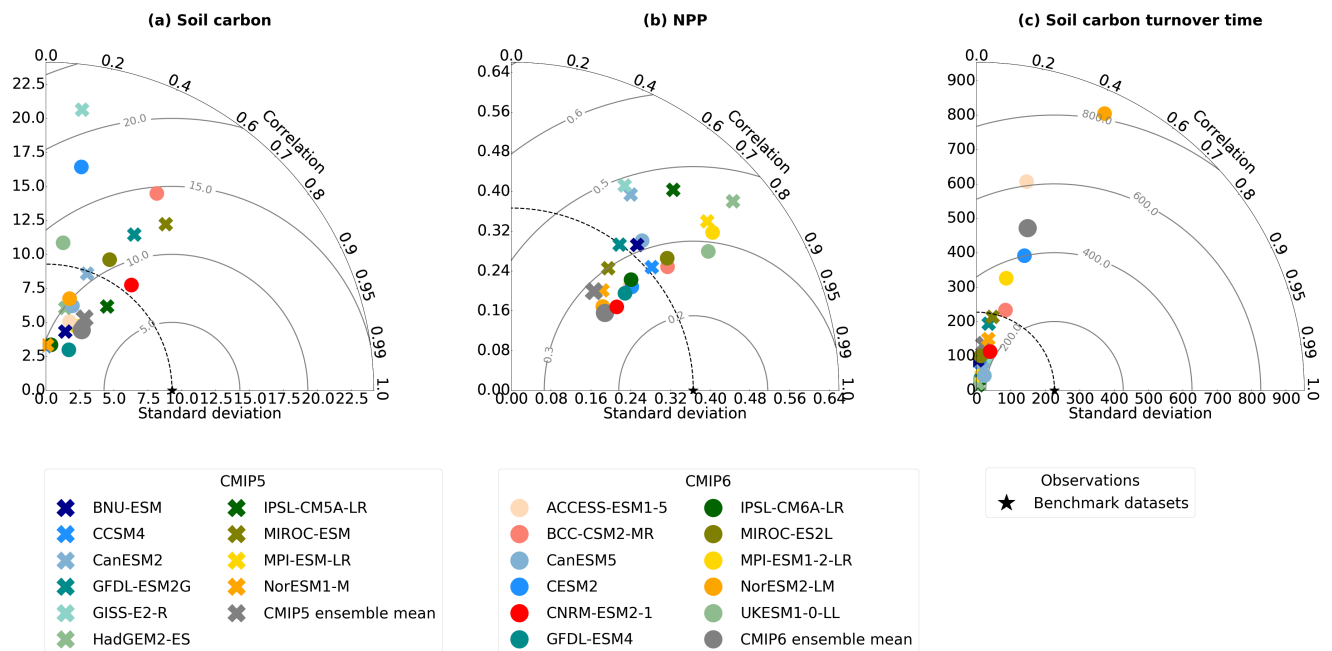


Figure 4. Taylor diagrams showing the spatial standard deviation (shown by the radial axis between standard x and y axes), the Pearson correlation coefficients (shown by the curved correlation axis), and the RMSE (show by the grey contours), for the ESMs in both CMIP5 and CMIP6 compared to the benchmark datasets, for (a) soil carbon (C_s), (b) NPP, and (c) soil carbon turnover time (τ_s).

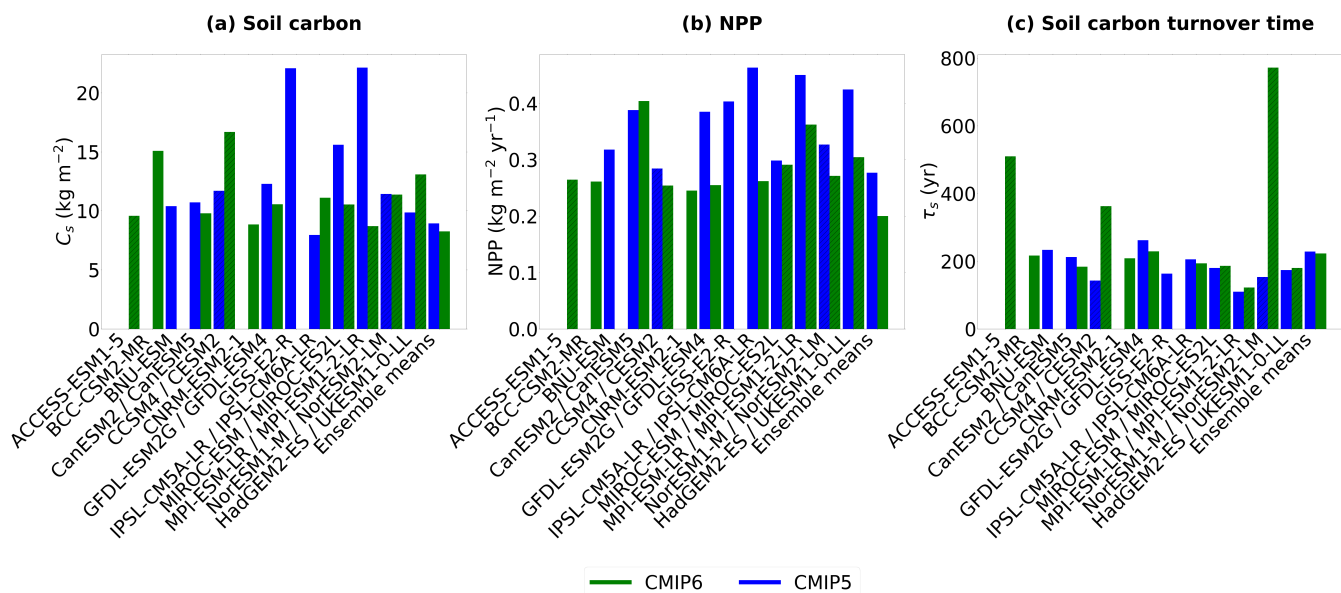


Figure 5. Bar charts comparing the Root Mean Squared Errors (RMSEs) in CMIP6 and CMIP5, for (a) soil carbon (C_s), (b) NPP, and (c) soil carbon turnover time (τ_s).

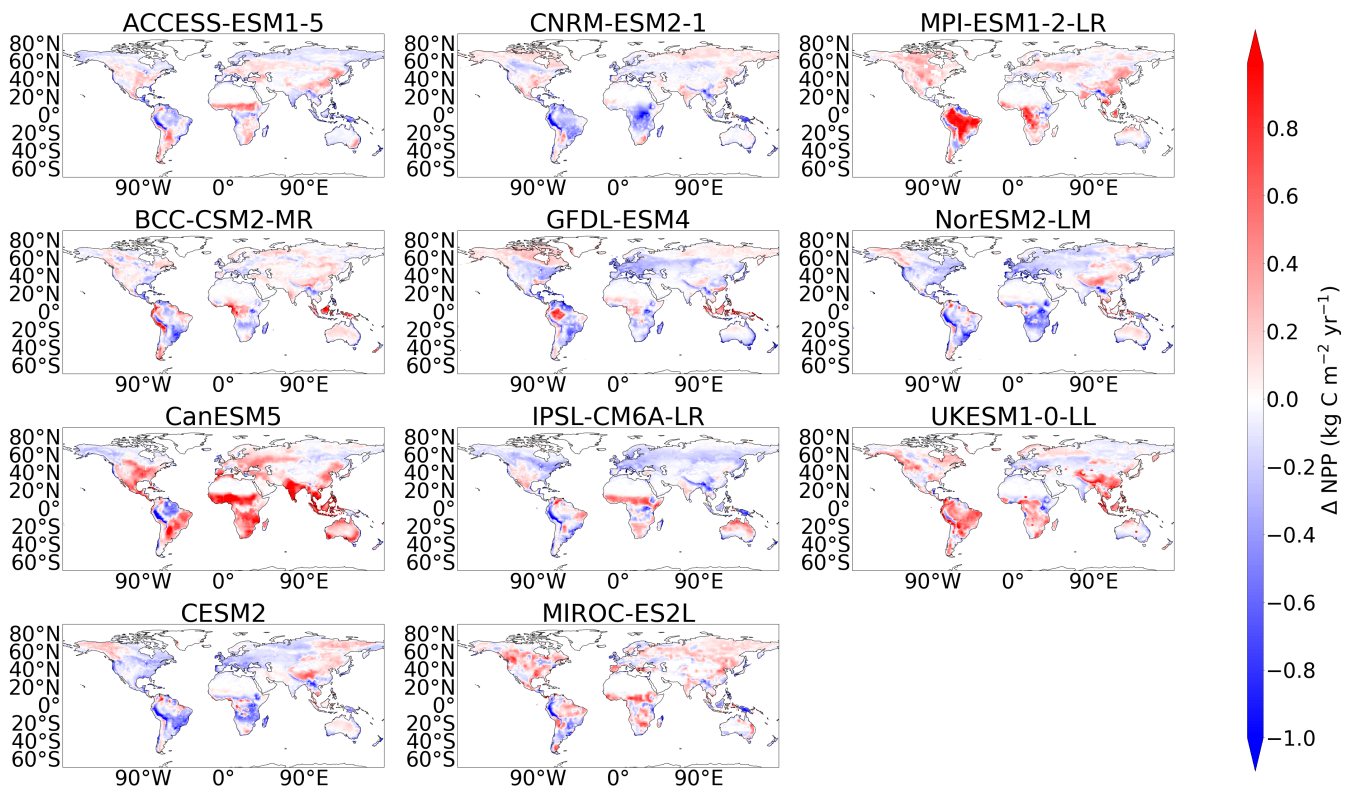


Figure 6. Maps of the difference in Net Primary Production (NPP) between the historical simulation of each CMIP6 model and the benchmark dataset.

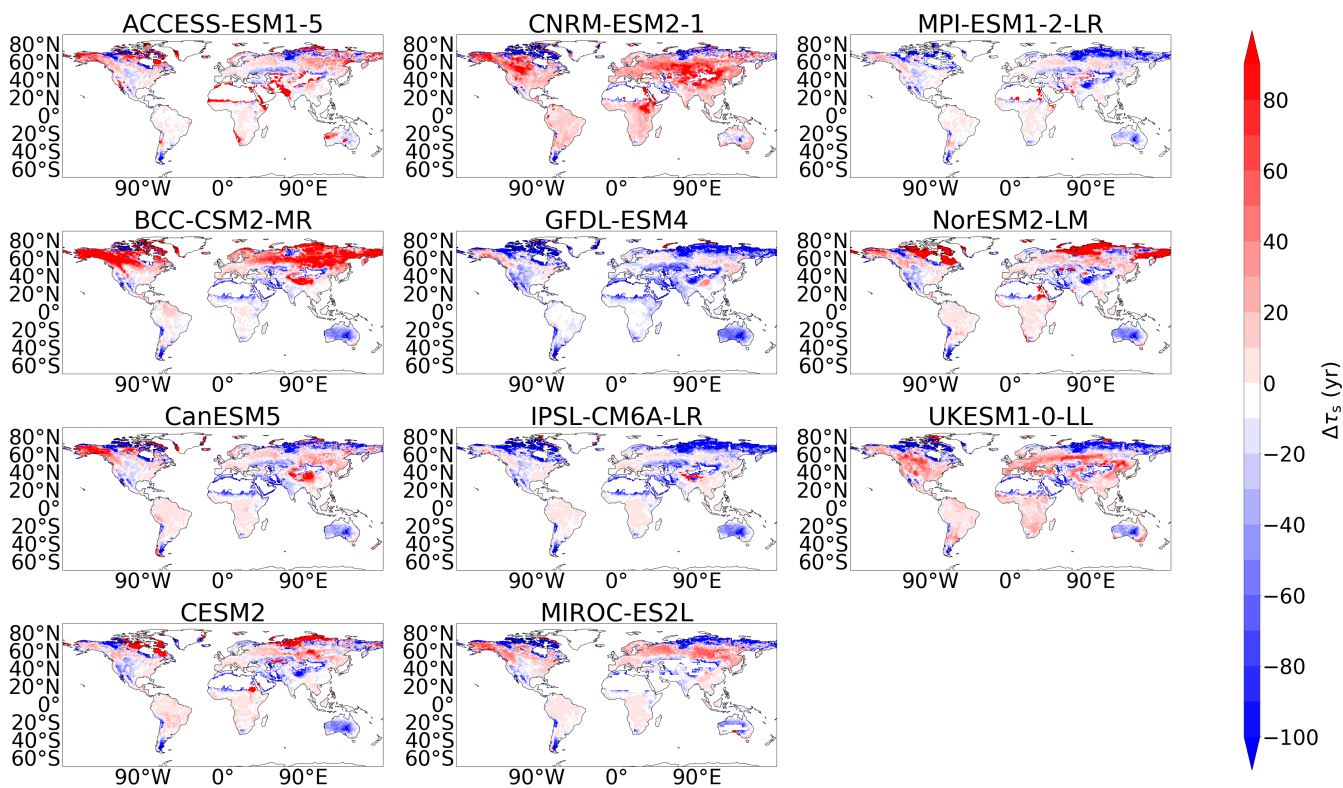


Figure 7. Maps of the difference in soil carbon turnover time (τ_s) between the historical simulation of each CMIP6 model and the benchmark datasets.

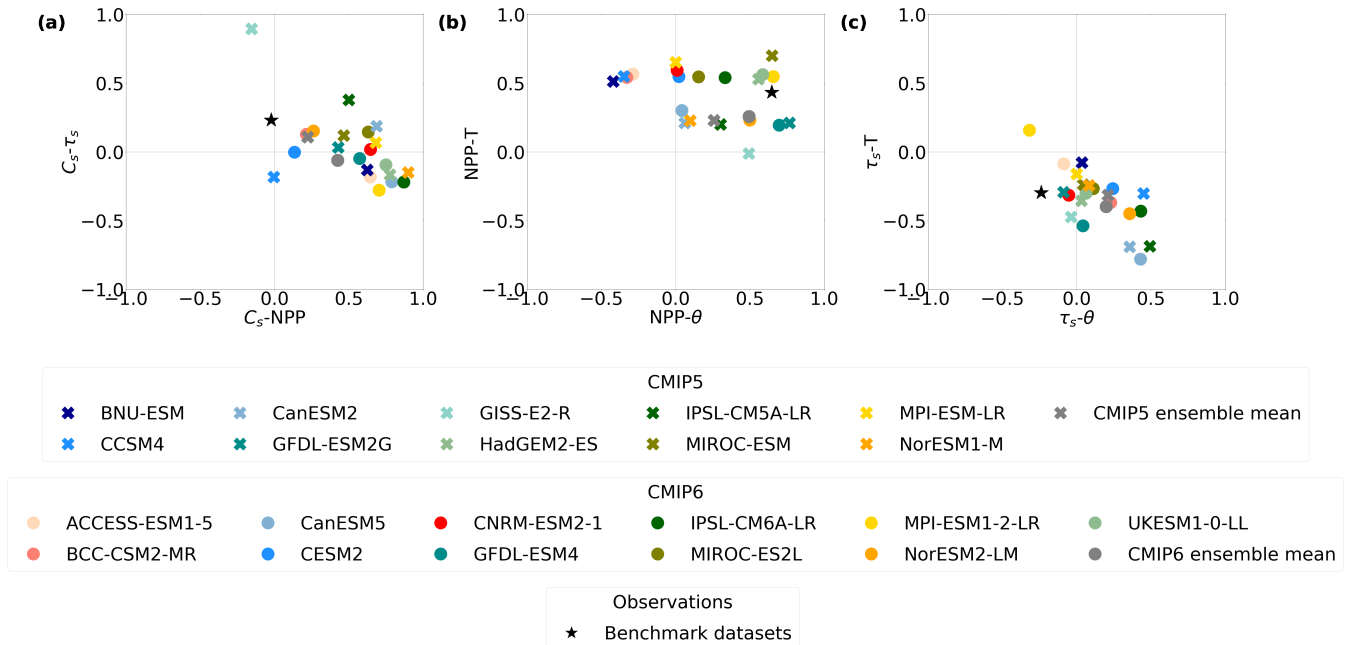


Figure 8. Scatter plots investigating the relationships between different Pearson correlation coefficients of climate variables, (a) C_s-T_s against C_s-NPP , (b) $NPP-T$ against $NPP-\theta$, (c) τ_s-T against $\tau_s-\theta$.

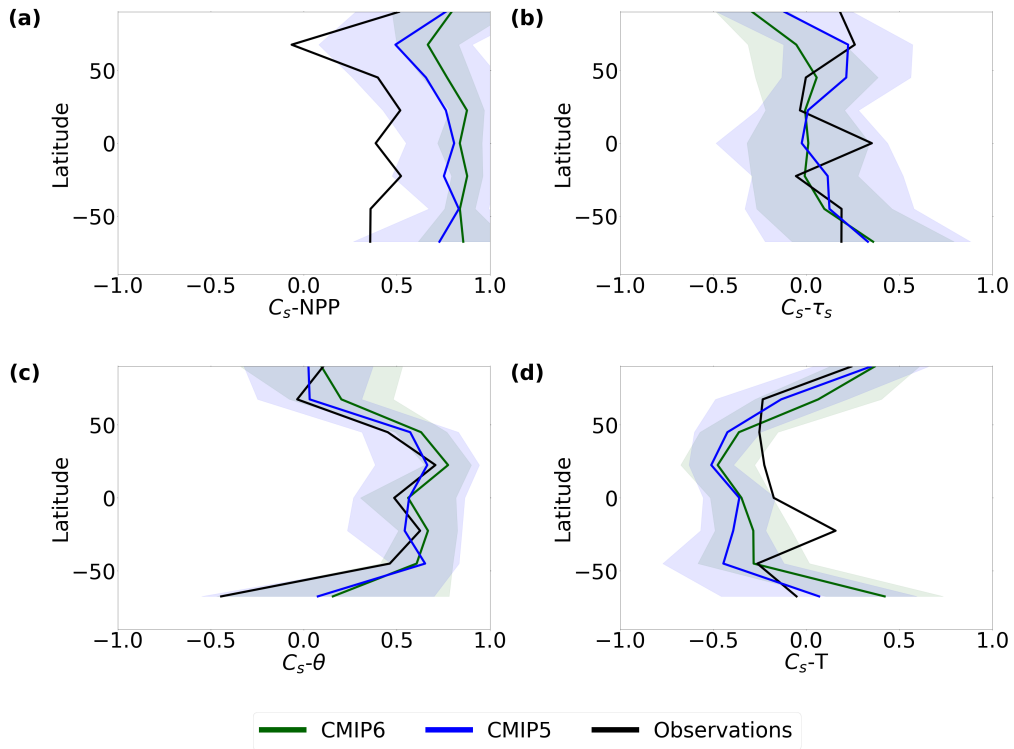


Figure 9. The latitudinal profiles of the Pearson correlation coefficients between soil carbon and (a) NPP (C_s -NPP), (b) soil carbon turnover time (C_s - τ_s), (c) soil moisture (C_s - θ), and (d) temperature (C_s -T).

Table 1. The 11 CMIP6 Earth System Models included in this study, and relevant features of their land carbon cycle components (Arora et al., 2020).

Earth System Model	Modelling Centre	Land Surface Model	Nitrogen cycle	No. of live carbon pools	No. of dead carbon pools	Temperature & Moisture	References
ACCESS-ESM1.5	CSIRO	CABLE2.4 + CASA-CNP	Yes	3	6	Arrhenius & Hill	Ziehn et al. (2020) Haverd et al. (2018) Trudinger et al. (2016)
BCC-CSM2-MR	BCC	BCC-AVIM2	No	3	8	Hill & Hill	Wu et al. (2019) Ji et al. (2008)
CanESM5	CCCma	CLASS-CTEM	No	3	2	Q_{10} & Hill	Swart et al. (2019) Melton et al. (2020) Seiler et al. (2021)
CESM2	CESM	CLM5	Yes	22	7	Arrhenius & Increasing	Danabasoglu et al. (2020) Lawrence et al. (2019)
CNRM-ESM2-1	CNRM	ISBA-CTRIP	No	6	7	Q_{10} & Increasing	S��ferian et al. (2019) Delire et al. (2020)
GFDL-ESM4	GFDL	LM4.1	No	6	4	Hill & Increasing	Dunne et al. (2020) Zhao et al. (2018)
IPSL-CM6A-LR	IPSL	ORCHIDEE branch 2.0	No	8	3	Q_{10} & Increasing	Boucher et al. (2020) Cheruy et al. (2020) Guimberteau et al. (2018)
MIROC-ES2L	JAMSTEC	MATSIRO VISIT-s	Yes	3	6	Arrhenius & Increasing	Hajima et al. (2020) Ito and Oikawa (2002)
MPI-ESM1.2-LR	MPI	JSBACH3.2	Yes	3	18	Q_{10} & Increasing	Mauritsen et al. (2019) Goll et al. (2017) Goll et al. (2015)
NorESM2-LM	NCC	CLM5	Yes	22	7	Arrhenius & Increasing	Seland et al. (2020) Lawrence et al. (2019)
UKESM1-0-LL	UK	JULES-ES-1.0	Yes	3	4	Q_{10} & Hill	Sellar et al. (2020) Wiltshire et al. (2021)

Table 2. The 10 CMIP5 Earth System Models included in this study, and relevant features of their land carbon cycle components (Arora et al., 2013; Anav et al., 2013; Friedlingstein et al., 2014). Including temperature and moisture functions presented in Todd-Brown et al. (2013).

Earth System Model	Modelling Centre	Land Surface Model	Nitrogen cycle	No. of live & dead carbon pools	Temperature & Moisture	References
BNU-ESM	BNU	CoLM + BNU-DGVM	Yes	-	Q_{10} & Increasing	Ji et al. (2014) Dai et al. (2003)
CCSM4	CCSM	CLM4	Yes	20	Arrhenius & Increasing	Gent et al. (2011) Lawrence et al. (2011)
CanESM2	CCCma	CLASS2.7 + CTEM1	No	5	Q_{10} & Hill	Arora et al. (2009) Arora and Boer (2010)
GFDL-ESM2G	GFDL	LM3	No	10	Hill & Increasing	Dunne et al. (2012) Dunne et al. (2013) Shevliakova et al. (2009)
GISS-E2-R	NASA-GISS	YIBs, version 1.0	No	12	Increasing & Increasing	Schmidt et al. (2014) Yue and Unger (2015)
HadGEM2-ES	MOHC	JULES + TRIFFID	No	7	Q_{10} & Hill	Jones et al. (2011) Best et al. (2011) Clark et al. (2011)
IPSL-CM5A-LR	IPSL	ORCHIDEE	No	7	Q_{10} & Increasing	Dufresne et al. (2013) Krinner et al. (2005)
MIROC-ESM	JAMSTEC	MATSIRO + SEIB-DGVM	No	6	Arrhenius & Increasing	Watanabe et al. (2011) Ito and Oikawa (2002) Sato et al. (2007)
MPI-ESM-LR	MPI	JSBACH + BETHY	No	6	Q_{10} & Increasing	Raddatz et al. (2007) Knorr (2000)
NorESM1-M	NCC	CLM4	Yes	20	Arrhenius & Increasing	Bentsen et al. (2013) Iversen et al. (2013) Lawrence et al. (2011)

Table 3. Table of global total and northern latitude total (northern latitudes defined as 60° N - 90° N) soil carbon estimates from multiple empirical datasets, for varying soil depths where applicable.

Empirical dataset	Depth	Global total C_s (PgC)	Northern latitude total C_s (PgC)	Reference
HWSD + NCSCD	1m	1412 ± 215	401 ± 61	FAO and ISRIC (2012) Hugelius et al. (2013)
WISE30sec	1m	1371 ± 129	314	Batjes (2016)
	2m	1952 ± 198	468	
S2017	1m	1966	515	Sanderman et al. (2017)
	2m	3141	893	
GSDE	1m	1682	526	Shangguan et al. (2014)
	2.3m	2593	849	
IGBP DIS	1m	1567	377	IGBP (2000)

Table 4. Table presenting global soil carbon values for the 11 CMIP6 models included in this study and the benchmark datasets. Including: global total C_s in PgC, and northern latitude total (90°N - 60°N) C_s in PgC, and the spatial mean value of C_s and corresponding standard deviation in kg m^{-2} .

Earth System Model	Global total C_s (PgC)	Northern latitude total C_s (PgC)	Mean $C_s \pm \text{std}$ (kg m^{-2})
ACCESS-ESM1.5	900	151	5.86 ± 5.35
BCC-CSM2-MR	1770	575	11.6 ± 16.6
CanESM5	1500	218	3.87 ± 6.52
CESM2 (cSoilAbove1m)	991	294	7.05 ± 16.6
<i>CESM2 (cSoil)</i>	<i>1870</i>	<i>1036</i>	<i>13.8 ± 51.7</i>
CNRM-ESM2-1	1810	440	12.2 ± 9.98
GFDL-ESM4	516	163	1.36 ± 3.43
IPSL-CM6A-LR	639	66.0	4.80 ± 3.37
MIROC-ES2L	1460	347	9.31 ± 10.7
MPI-ESM1.2-LR	970	175	6.68 ± 5.23
NorESM2-LM (cSoilAbove1m)	969	300	2.61 ± 6.97
<i>NorESM2-LM (cSoil)</i>	<i>2430</i>	<i>1563</i>	<i>6.60 ± 41.3</i>
UKESM1-0-LL	1760	194	12.0 ± 10.9
Ensemble mean	1206 ± 445	266 ± 139	2.80 ± 5.15
Benchmark dataset	1412 ± 215	401 ± 83	10.7 ± 9.28

Table 5. Table presenting global soil carbon values for the 10 CMIP5 models included in this study and the benchmark datasets. Including: global total C_s in PgC, and northern latitude total (90°N - 60°N) C_s in PgC, and the spatial mean value of C_s and corresponding standard deviation in kg m^{-2} .

Earth System Model	Global total C_s (PgC)	Northern latitude total C_s (PgC)	Mean $C_s \pm \text{std}$ (kg m^{-2})
BNU-ESM	681	135	5.31 ± 4.55
CCSM4	507	28.1	4.03 ± 3.24
CanESM2	1540	300	9.16 ± 9.11
GFDL-ESM2G	1420	635	9.47 ± 13.2
GISS-E2-R	2150	609	15.9 ± 20.8
HadGEM2-ES	1080	148	8.19 ± 6.24
IPSL-CM5A-LR	1350	346	9.77 ± 7.64
MIROC-ESM	2550	742	20.5 ± 15.1
MPI-ESM-LR	3000	204	23.5 ± 14.8
NorESM1-M	538	31.0	3.61 ± 3.34
Ensemble mean	1480 ± 810	318 ± 246	10.5 ± 6.02
Benchmark dataset	1412 ± 215	401 ± 83	10.7 ± 9.28

Table 6. Table presenting global carbon fluxes and turnover time values for the 11 CMIP6 models included in this study and the benchmark datasets. Including: global total NPP (PgC yr^{-1}) and effective average soil carbon turnover time (yr).

Earth System Model	NPP (PgC yr^{-1})	τ_s (yr)
ACCESS-ESM1.5	45.6	19.0
BCC-CSM2-MR	51.2	34.1
CanESM5	75.5	18.1
CESM2 (cSoilAbove1m)	43.9	25.8
<i>CESM2 (cSoil)</i>	-	50.4
CNRM-ESM2-1	45.6	41.5
GFDL-ESM4	52.6	11.2
IPSL-CM6A-LR	46.4	14.6
MIROC-ES2L	59.1	24.5
MPI-ESM1.2-LR	58.9	15.4
NorESM2-LM (cSoilAbove1m)	43.5	24.0
<i>NorESM2-LM (cSoil)</i>	-	60.8
UKESM1-0-LL	60.8	28.1
Ensemble mean	53.0 ± 9.39	23.3 ± 8.59
Benchmark datasets	56.6 ± 14.3	27.0^{+27}_{-11}

Table 7. Table presenting global carbon fluxes and turnover time values for the 10 CMIP5 models included in this study and the benchmark datasets. Including: global total NPP (PgC yr^{-1}) and effective average soil carbon turnover time (yr).

Earth System Model	NPP (PgC yr^{-1})	τ_s (yr)
BNU-ESM	44.3	16.6
CCSM4	42.9	14.3
CanESM2	59.0	72.9
GFDL-ESM2G	74.4	57.3
GISS-E2-R	31.0	47.1
HadGEM2-ES	69.1	16.8
IPSL-CM5A-LR	76.6	19.4
MIROC-ESM	47.1	56.8
MPI-ESM-LR	73.5	42.7
NorESM1-M	45.0	34.5
Ensemble mean	56.3 ± 15.4	37.8 ± 19.7
Benchmark datasets	56.6 ± 14.3	27.0^{+27}_{-11}

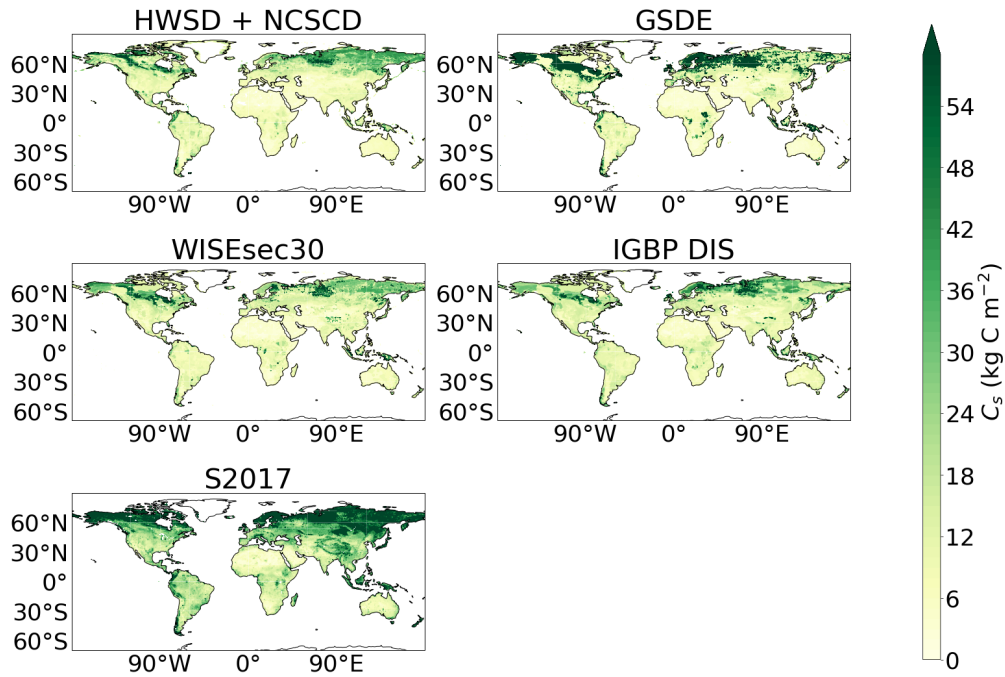


Figure A1. Maps comparing empirical datasets of soil carbon (C_s). The benchmark dataset is a map plot showing C_s approximated to a depth of 1m by combining the Harmonized World Soils Database (HWSD) (FAO and ISRIC, 2012) and Northern Circumpolar Soil Carbon Database (NCSCD) (Hugelius et al., 2013), where NCSCD was used where overlap occurs. Additional map plots are shown for empirical C_s estimated by: the World Inventory of Soil property Estimates (WISE30sec) (Batjes, 2016), the named ‘S2017’ from Sanderman et al. (2017), the Global Soil Dataset for use in Earth System Models (GSDE) (Shangguan et al., 2014), and the Global Gridded Surfaces of Selected Soil Characteristics (IGBP-DIS) (IGBP, 2000).

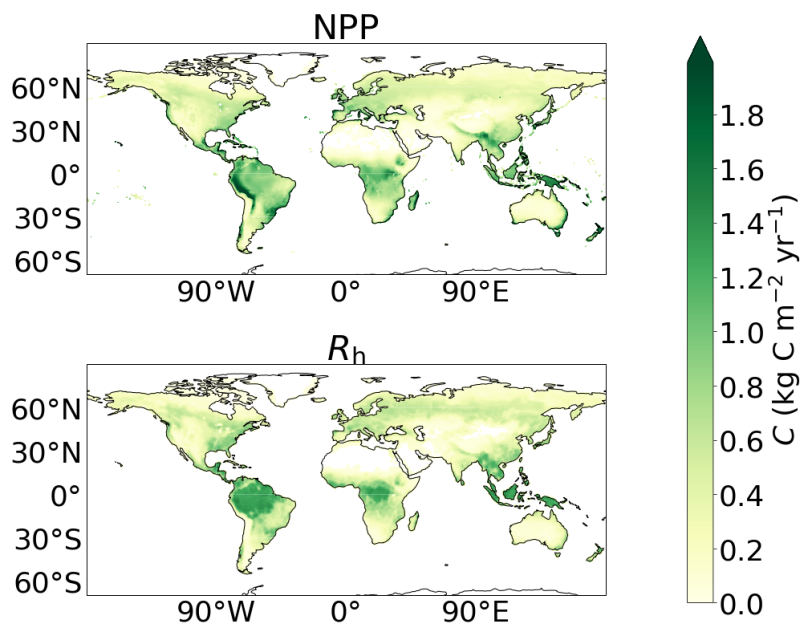


Figure A2. Maps of empirical carbon flux datasets. Net Primary Production (NPP) is approximated using the MODIS NPP dataset (Zhao et al., 2005), and Heterotrophic Respiration (R_h) is approximated using the CARDAMOM R_h dataset (Bloom et al., 2015).

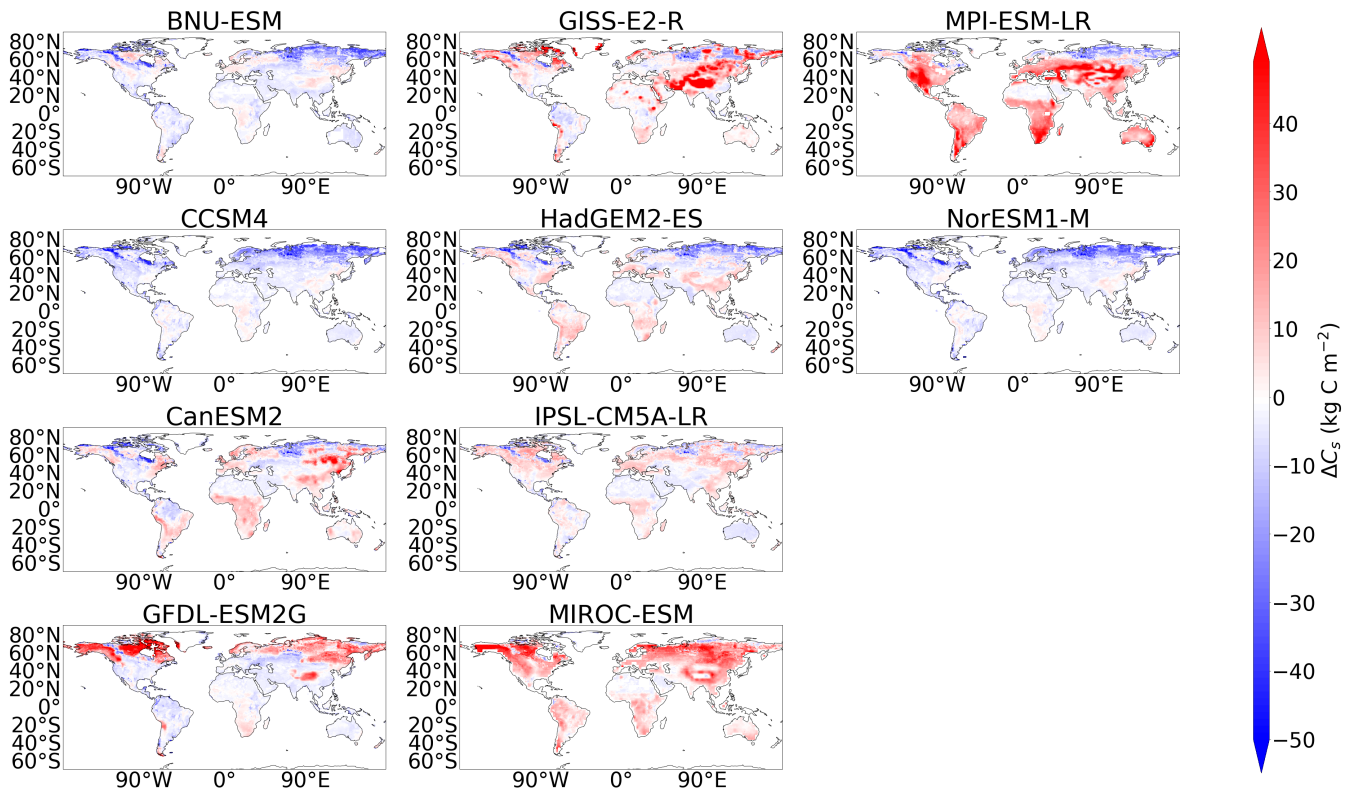


Figure A3. Maps of the difference in soil carbon (C_s) between the historical simulation (1950-2000) for the CMIP5 models and the benchmark dataset.

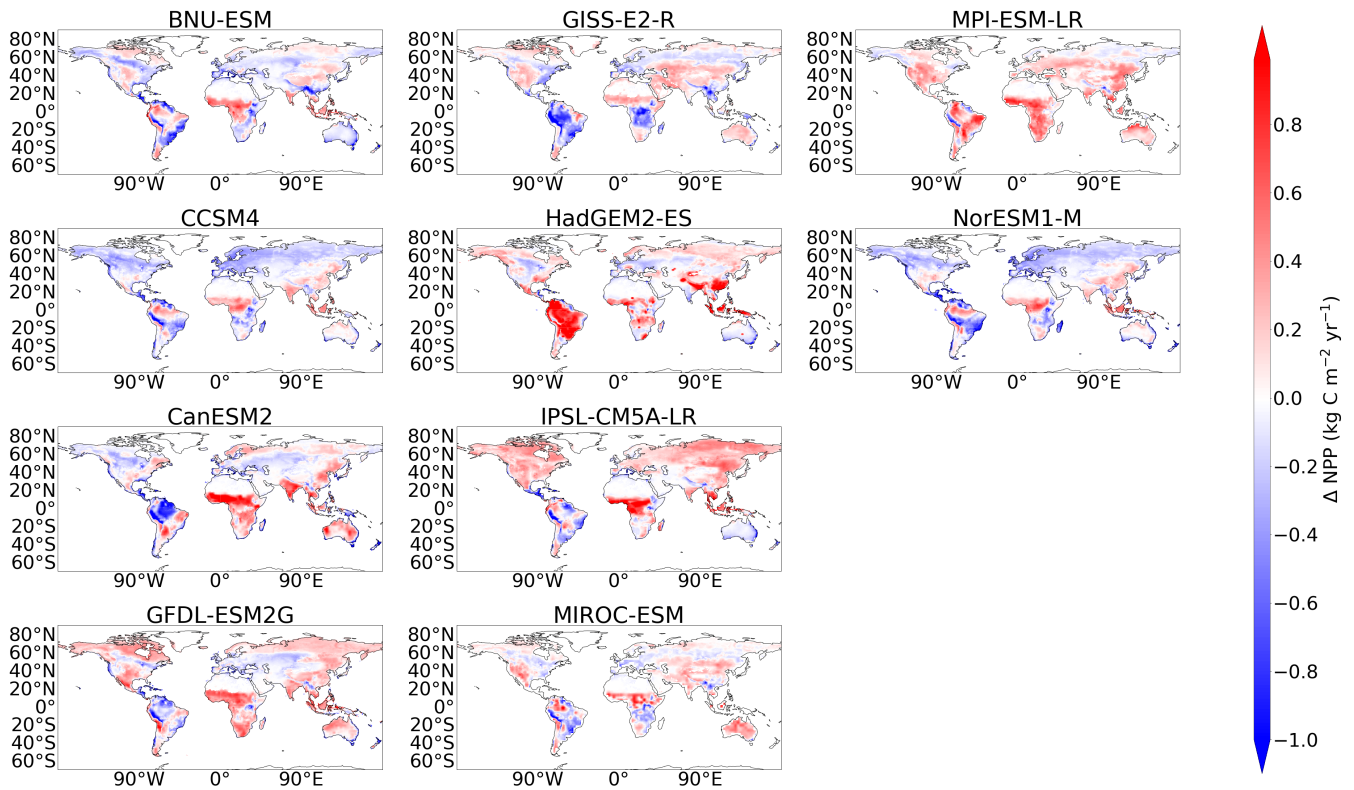


Figure A4. Maps of the difference in NPP between the historical simulation (1995-2005) for the CMIP5 models and the benchmark dataset.

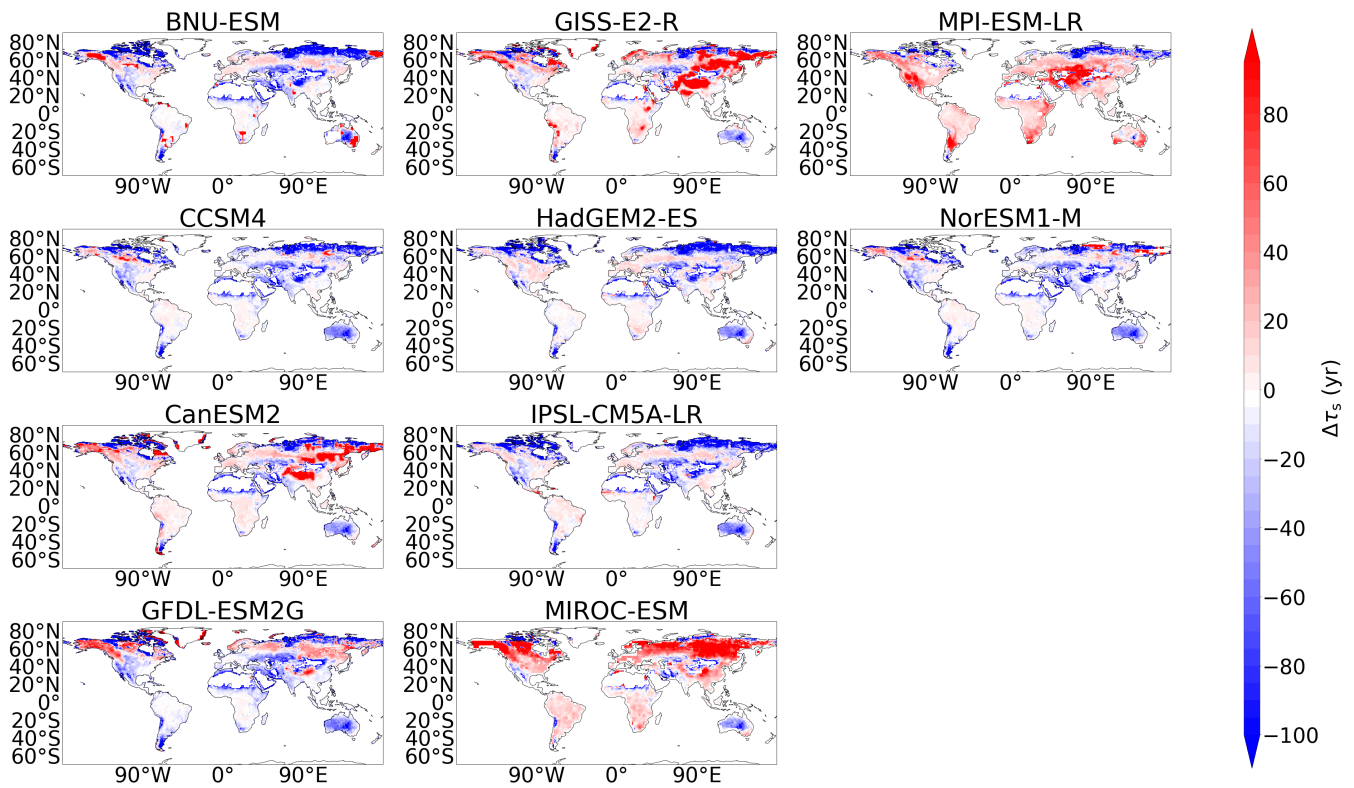


Figure A5. Maps of the difference in τ_s between the historical simulation for the CMIP5 models and the benchmark datasets, where τ_s is defined as the ratio of C_s (1950-2000) to R_h (1995-2005).

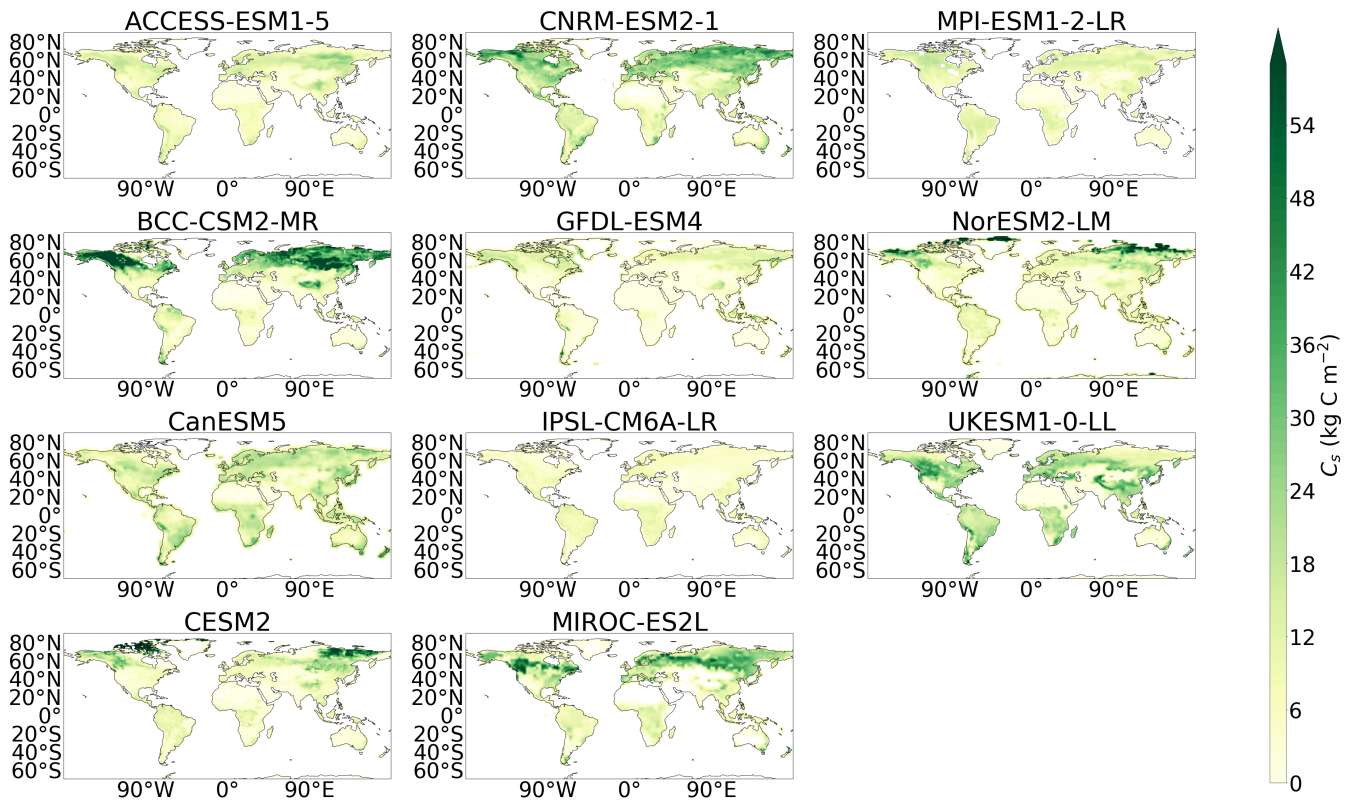


Figure A6. Maps of soil carbon (C_s) in the historical simulation (1950-2000) for the CMIP6 models.

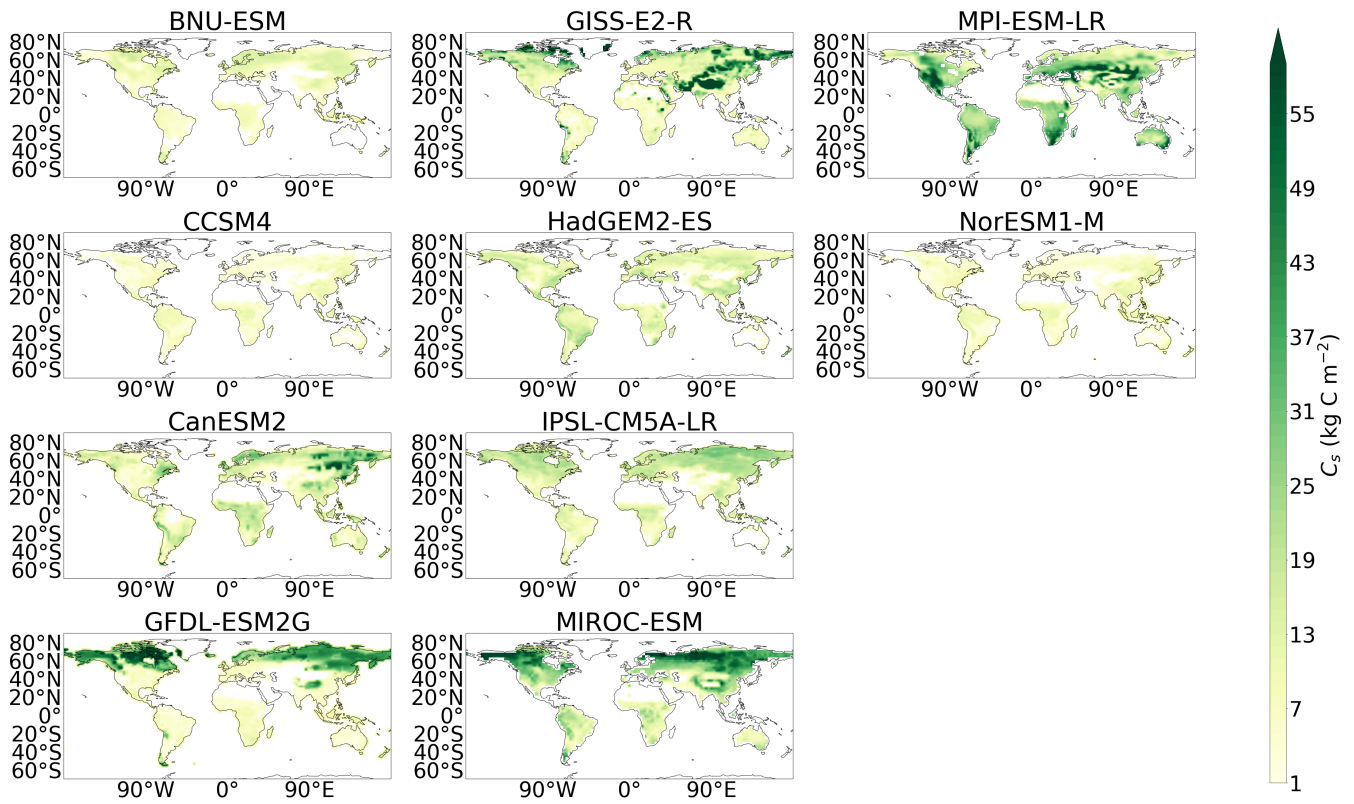


Figure A7. Maps of soil carbon (C_s) in the historical simulation (1950-2000) for the CMIP5 models.

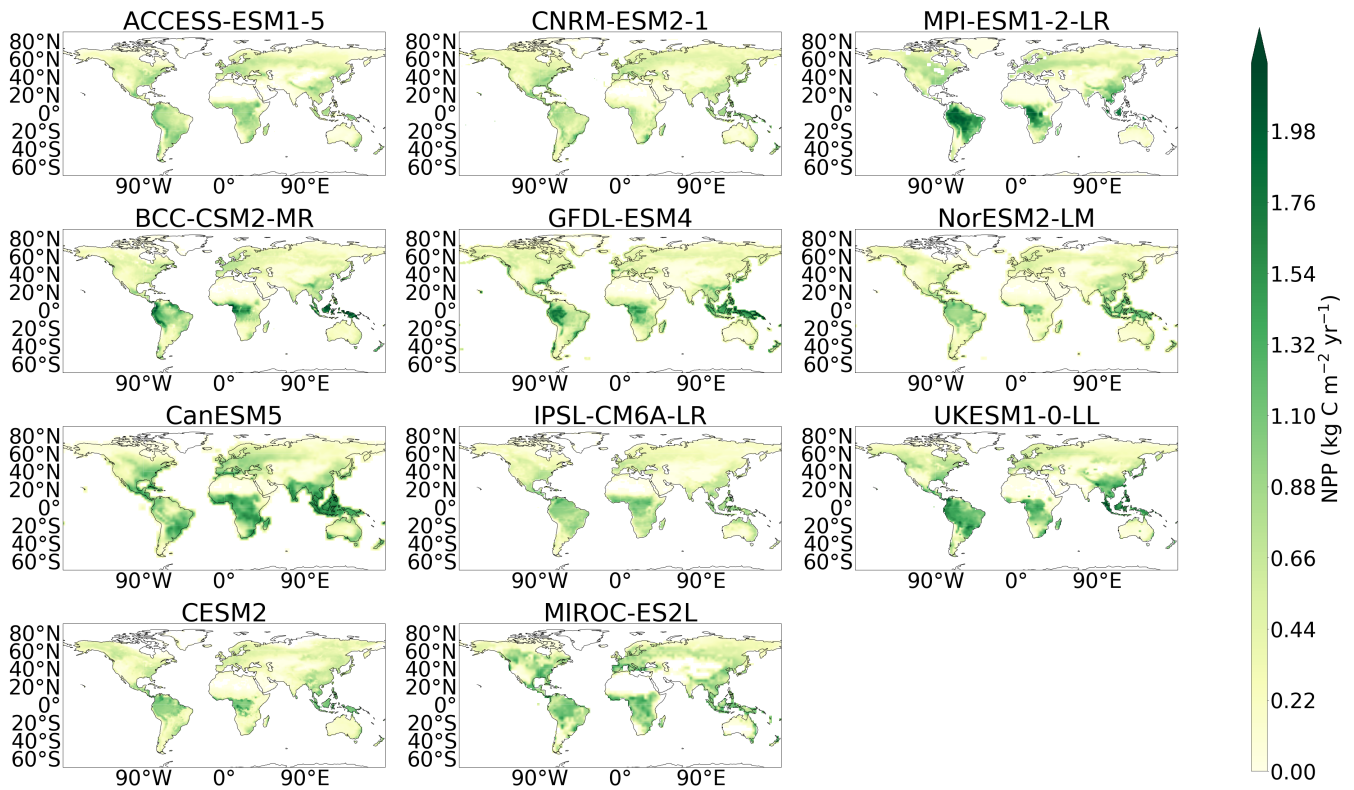


Figure A8. Maps of Net Primary Productivity (NPP) in the historical simulation (1995-2005) for the CMIP6 models.

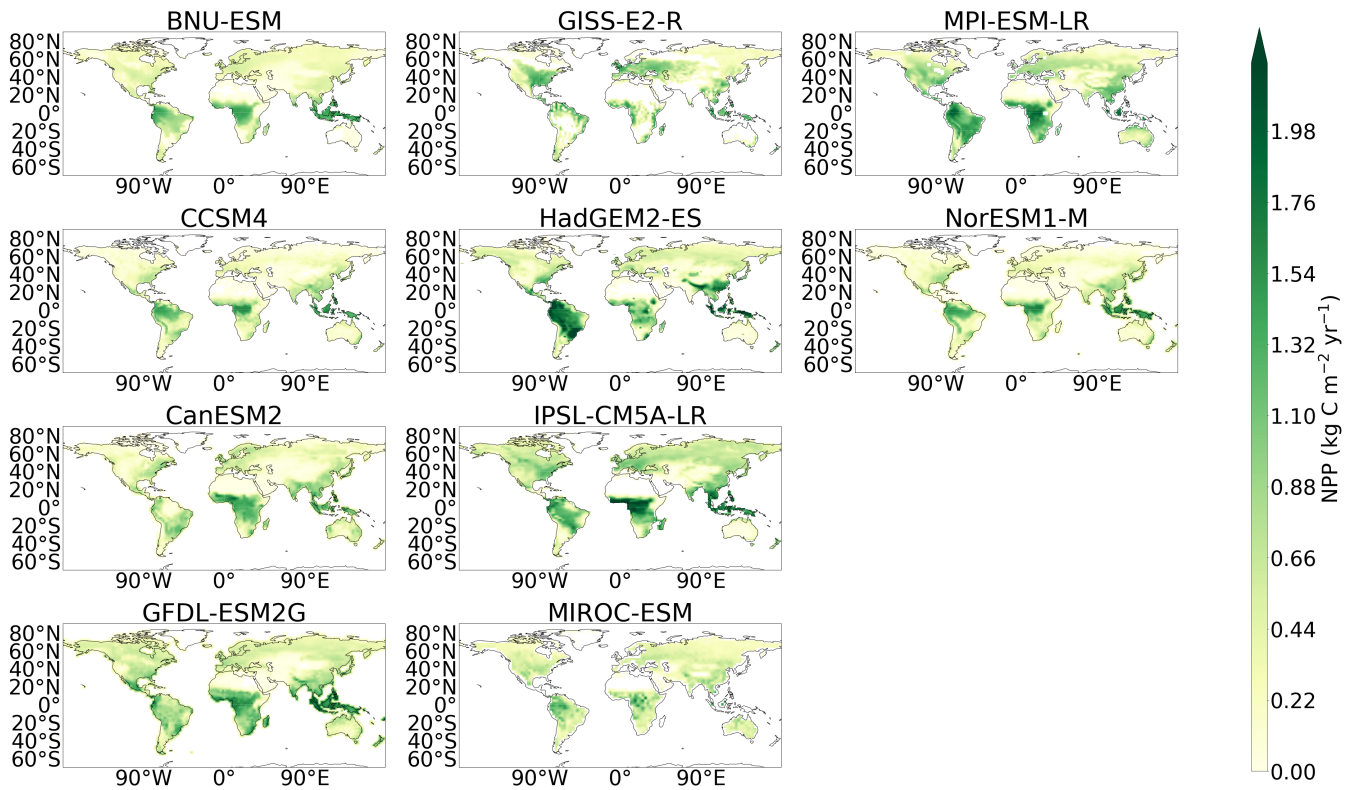


Figure A9. Maps of Net Primary Productivity (NPP) in the historical simulation (1995-2005) for the CMIP5 models.

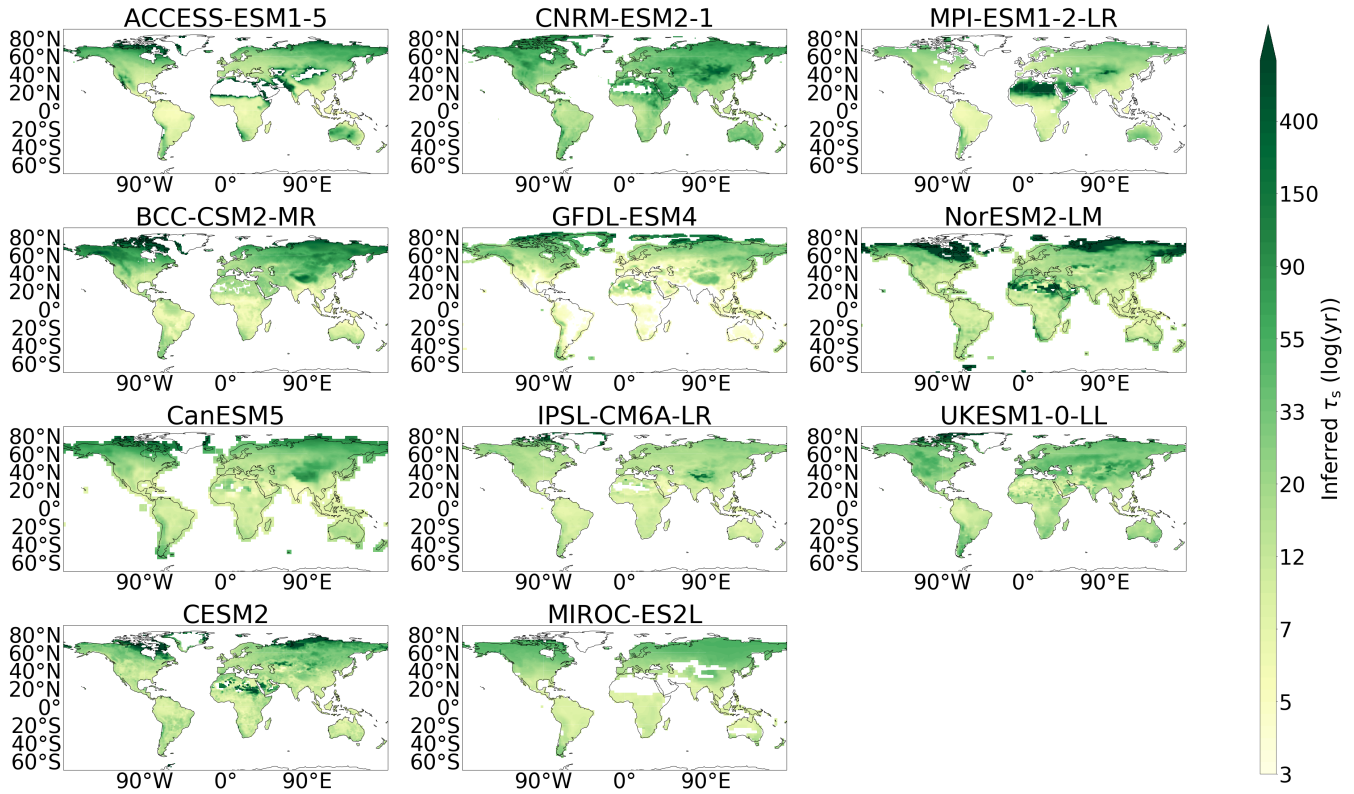


Figure A10. Maps of soil carbon turnover times (τ_s) in the historical simulation for the CMIP6 models, where τ_s is defined as the ratio of C_s (1950-2000) to R_h (1995-2005).

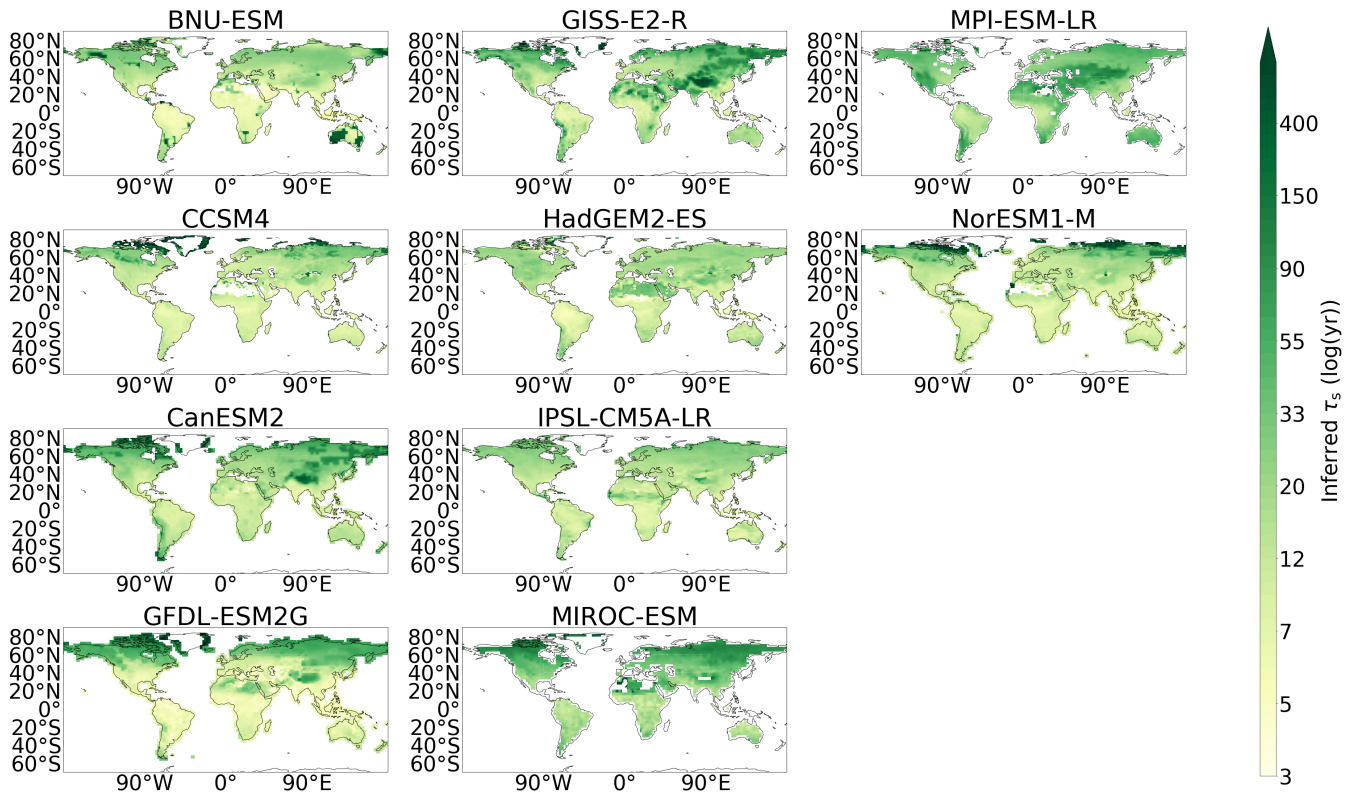


Figure A11. Maps of soil carbon turnover times (τ_s) in the historical simulation for the CMIP5 models, where τ_s is defined as the ratio of C_s (1950-2000) to R_h (1995-2005).

Table A1. Table presenting global carbon fluxes (PgC yr^{-1}), NPP and R_h , for the 11 CMIP6 models included in this study and the empirical benchmark datasets.

Earth System Model	NPP (PgC yr^{-1})	R_h (PgC yr^{-1})
ACCESS-ESM1.5	45.6	45.1
BCC-CSM2-MR	51.2	48.9
CanESM5	75.5	75.0
CESM2	43.9	38.3
CNRM-ESM2-1	45.6	40.3
GFDL-ESM4	52.6	43.7
IPSL-CM6A-LR	46.4	39.9
MIROC-ES2L	59.1	52.7
MPI-ESM1.2-LR	58.9	53.4
NorESM2-LM	43.5	38.2
UKESM1-0-LL	60.8	57.5
Ensemble mean	53.0 ± 9.39	48.4 ± 10.5
Benchmark datasets	56.6 ± 14.3	51.7 ± 21.8

Table A2. Table presenting global carbon fluxes (PgC yr^{-1}), NPP and R_h , for the 10 CMIP5 models included in this study and the empirical benchmark datasets.

Earth System Model	NPP (PgC yr^{-1})	R_h (PgC yr^{-1})
BNU-ESM	44.3	42.5
CCSM4	42.9	41.4
CanESM2	59.0	58.8
GFDL-ESM2G	74.4	62.7
GISS-E2-R	31.0	39.5
HadGEM2-ES	69.1	67.0
IPSL-CM5A-LR	76.6	62.4
MIROC-ESM	47.1	41.2
MPI-ESM-LR	73.5	59.9
NorESM1-M	45.0	41.3
Ensemble mean	56.3 ± 15.4	52.8 ± 10.7
Benchmark datasets	56.6 ± 14.3	51.7 ± 21.8